Formation of stable mixed guanidinium-methylammonium phases with exceptionally long carrier lifetimes for high efficiency lead iodide-based perovskite photovoltaics

Dominik J. Kubicki,[a†] Daniel Prochowicz,[b,c†] Albert Hofstetter,[a] Marcin Saski,[c] Pankaj Yadav,[b,d] Dong-qin Bi,[b] Norman Pellet,[b] Janusz Lewiński,*[c] Shaik M. Zakeeruddin,[b] Michael Grätzel,*[b] Lyndon Emsley*[a]

[a]*Laboratory of Magnetic Resonance, Institute of Chemical Sciences and Engineering, Ecole Polytechnique Fédérale de Lausanne (EPFL), CH-1015 Lausanne, Switzerland*
[b]*Laboratory of Photonics and Interfaces, Institute of Chemical Sciences and Engineering, Ecole Polytechnique Fédérale de Lausanne (EPFL), CH-1015 Lausanne, Switzerland*
[c]*Institute of Physical Chemistry, Polish Academy of Sciences, Kasprzaka 44/52, 01-224 Warsaw, Poland.*
[d]*School of Technology, Pandit Deendayal Petroleum University, Gandhinagar 382 007, Gujarat*

Supporting Information Placeholder

ABSTRACT: Methylammonium (MA)- and formamidinium (FA)-based organic-inorganic lead halide perovskites provide outstanding performance as photovoltaic materials, due to their versatility of fabrication and their power conversion efficiencies reaching over 22%. The proposition of guanidinium (GUA)-doped perovskite materials generated considerable interest due to their potential to increase carrier lifetimes and open circuit voltages as compared to pure $MAPbI_3$. However, simple size considerations based on the Goldshmidt tolerance factor suggest that guanidinium is too big to replace methylammonium as an A cation in the $APbI_3$ perovskite lattice, and its effect was thus ascribed to passivation of surface trap states at grain boundaries. As guanidinium was not thought to incorporate into the $MAPbI_3$ lattice, interest waned since it appeared unlikely that it could be used to modify the intrinsic perovskite properties. Here, using solid-state NMR, we show that not only is GUA directly incorporated into the $MAPbI_3$ and $FAPbI_3$ lattices, forming pure $GUA_xMA_{1-x}PbI_3$ or $GUA_xFA_{1-x}PbI_3$ phases, but we also find that it reorients on the picosecond timescale within the perovskite lattice, which explains its superior charge carrier stabilisation capacity. Our findings establish a fundamental link between charge carrier lifetimes observed in photovoltaic perovskites and the A cation structure in ABX_3 type metal halide perovskites.

Introduction

Perovskite-based photovoltaics (PV) are developing very rapidly due to their potential to replace silicon solar cells in many applications, where they have, for example, the advantage of easy solution processing. Many different compositions have been proposed recently, with the highest photovoltaic efficiencies (PCE) being reported for mixed-cation lead halides, featuring methylammonium (MA), formamidinium (FA), caesium and rubidium as A cations.[1-10] A key metric is the lifetime of the intrinsic photo-generated charge carriers, which determines the charge carrier diffusion length[11] and, in particular, the open circuit voltage (V_{OC}) of the device, as longer lifetimes imply a reduction in the rate of radiation-less recombination processes resulting in a higher solar-to-electric power conversion efficiency (PCE).[11]

Guanidinium ($C(NH_2)_3^+$, (GUA)), has been proposed as an attractive candidate for an A cation in $APbI_3$-type perovskites before, based on theoretical predictions,[12] and initial PV data with guanidinium-doped $MAPbI_3$ [13-14] On its own, guanidinium forms a yellow $GUAPbI_3$ phase which is photoinactive,[15] hence the idea of incorporating it into a pre-existing 3D perovskite lattice of $MAPbI_3$ or $FAPbI_3$, the current gold standard perovskite PV materials. The analysis of the Goldschmidt tolerance factors indicates that it should be possible to formulate mixed-cation MA/GUA and FA/GUA lead iodide phases (Table S1). Yang *et al.* reported promising result with guanidinium-containing $MAPbI_3$ showing a factor of 10 or 2.5 longer charge carrier lifetime compared to pure $MAPbI_3$, as measured by time-resolved photoluminescence (TRPL) and photovoltage decay, respectively.[13] However they attributed the result to surface passivation of an unmodified pure $MAPbI_3$ phase by a layer of $GUAPbI_3$. Another study obtained 3.5 longer charge carrier lifetimes, measured by TRPL and attributed this enhancement to the same cause.[14]

Charge carriers in PV perovskites have been shown to be polaronic in nature, i.e. dominated by a strong stabilising interaction with the reorienting cation.[16-17] We have recently quantified the extent of this stabilisation by linking charge carrier lifetimes to the reorientation rate of MA and FA in the perovskite cages of mixed-cation materials, with faster cation reorientation leading to enhanced stabilisation and slower charge recombination.[18]

Applying for the first time solid-state magic angle spinning (MAS) nuclear magnetic resonance (NMR) to address this key question we show here that, despite its size, guanidinium is readily accommodated on A cation sites within the 3D perovskite structure of $MAPbI_3$ and $FAPbI_3$, forming a pure $GUA_xMA_{1-x}PbI_3$ or $GUA_xFA_{1-x}PbI_3$ phase. Moreover, we show that the GUA cation undergoes rapid reorientation on the picosecond timescale in these structures, which leads to charge carrier stabilisation through the electron-rotor interaction,[19] and to record

long charge carrier lifetimes on the order of 3 µs, as measured by time-resolved photoluminescence.

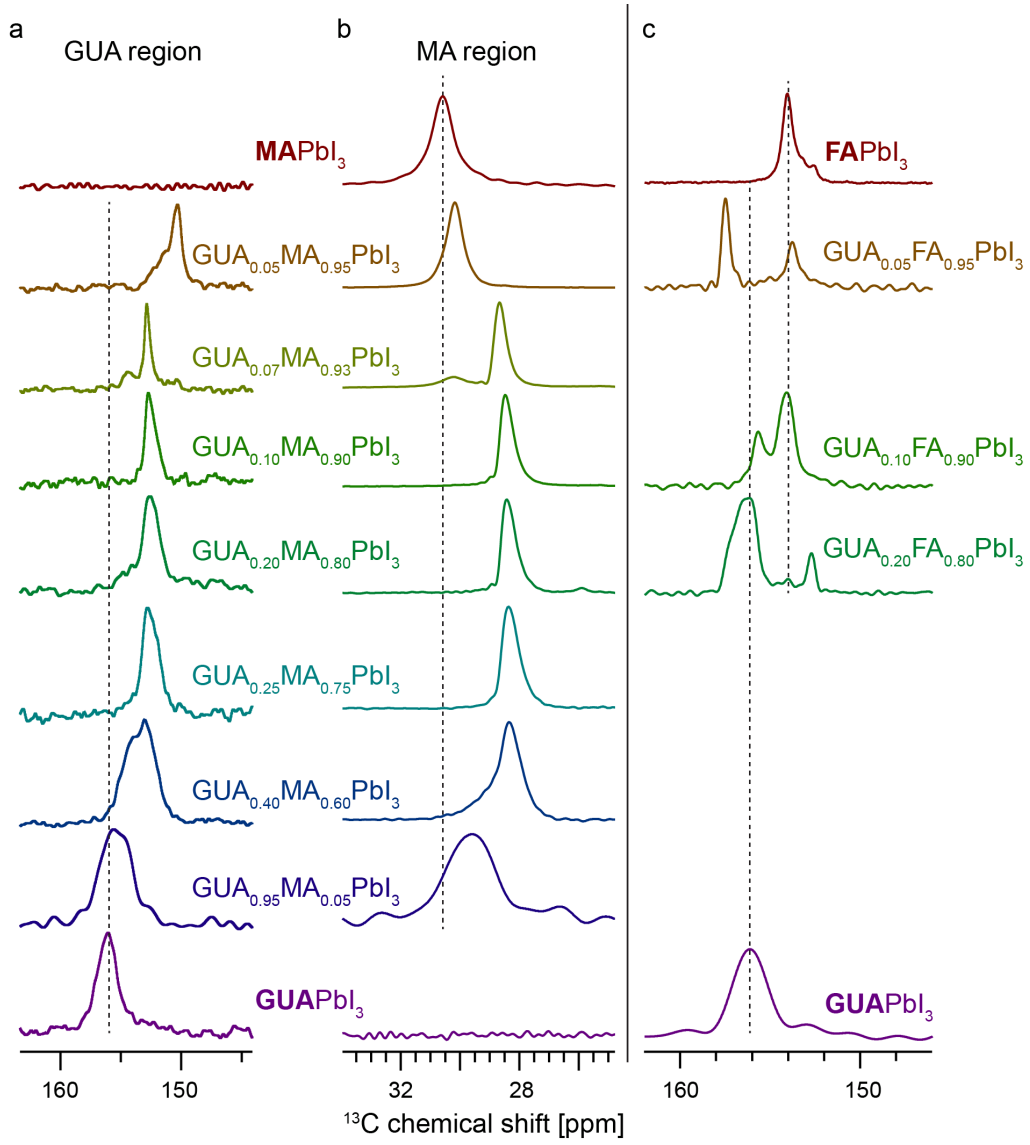

Figure 1. Low-temperature (100 ± 3 K) ^{13}C CP MAS spectra of (a,b) $GUA_xMA_{1-x}PbI_3$, and (c) $GUA_xFA_{1-x}PbI_3$ compositions. (a) and (b) show the GUA and the MA chemical shift ranges, respectively (signal intensities have been normalised). Dashed lines indicate chemical shifts of pure single-cation phases. The full spectra are reported in fig. S13 and S14.

Experimental

Materials. The following materials were used: guanidinium hydroiodide (TCI, 99.95%), methylammonium iodide (DyeSol), PbI_2 (TCI, 99.99%), D_2O (Sigma, 99.9 atom% D).

Mechanosynthesis of mixed guanidinium-methylammonium lead iodides ($GUA_xMA_{1-x}PbI_3$). All reagents were ground under an argon atmosphere. 0.009 g of GUA (0,05 mmol), 0.151 g of MA (0.95 mmol) and 0.461 g of PbI_2 (1.00 mmol) were ground to prepare $GUA_{0.05}MA_{0.95}PbI_3$ (black powder). 0.018 g of GUA·HI (0,10 mmol), 0.143 g of MA·HI (0.90 mmol) and 0.461 g of PbI_2 (1.00 mmol) were ground to prepare $GUA_{0.10}MA_{0.90}PbI_3$ (black powder). 0.046 g of GUA·HI (0.25 mmol), 0.119 g of MA·HI (0.75 mmol) and 0.461 g of PbI_2 (1.00 mmol) were ground to prepare $GUA_{0.25}MA_{0.75}PbI_3$ (black powder). 0.074 g of GUA·HI (0.40 mmol), 0.095 g of MA·HI (0.60 mmol) and 0.461 g of PbI_2 (1.00 mmol) were ground to prepare $GUA_{0.40}MA_{0.60}PbI_3$ (black powder). Other GUA/MA compositions were prepared analogously. 0.187 g of GUA·HI (1.0 mmol) and 0.461 g of PbI_2 (1.00 mmol) were ground to prepare $GUAPbI_3$ (pale-yellow powder). $GUA(d_6)PbI_3$ and $GUA(d_6)_{0.25}MA_{0.75}PbI_3$ were made analogously, using guanidinium hydroiodide N-deuterated by exchange with heavy water. After milling, the resulting powders were annealed at 110 °C for 10 minutes. In quantifying the stoichiometry of the mixed-cation compositions we relied on the amount of reagents taken to the reaction (measured to within ±0.5 mg) since the perovskites obtained in a mechanochemical reaction were used without any further processing (apart from mild annealing), excluding the possibility of modifying the GUA/MA ratio. All compositions were characterized using powder X-ray diffraction, as described in the SI.

Mechanosynthesis of mixed guanidinium-formamidinium lead iodides ($GUA_xFA_{1-x}PbI_3$). 0.037 g of GUA·HI (0.20

mmol), 0.137 g of FA·HI (0.80 mmol) and 0.461 g of PbI_2 (1.00 mmol) were ground under an argon atmosphere to prepare the $GUA_{0.20}FA_{0.80}PbI_3$. After milling, the resulting powders were annealed at 140°C for 10 minutes. Other GUA/FA compositions were prepared analogously. All compositions were characterized using powder X-ray diffraction, as described in the SI.

Deuteration of guanidinium hydroiodide (GUA·HI). GUA·HI was mixed with D_2O in a 1:40 mol/mol ratio, followed by evaporation using a rotary evaporator. The operation was repeated five times. The final product was dried in a vacuum oven at 100°C overnight.

NMR measurements. Variable-temperature ^{13}C (125.7 MHz), ^{2}H (76.8 MHz) and ^{14}N (32.1 MHz) NMR spectra were acquired on a Bruker Avance III 11.7 T spectrometer equipped with a 3.2 mm low-temperature CPMAS probe. Further acquisition details are given in Table S3.

$GUA_{0.25}MA_{0.75}PbI_3$ thin film preparation. A precursor solution was prepared by dissolving 0.065 g of GUA·HI, 0.167 g of MA·HI and 0.645 g of PbI_2 in 1 mL of anhydrous DMSO. The solution was then deposited onto a glass substrate (3.5 cm^2) by spin coating in a two-step program at 1000 and 6000 rpm for 10 and 20 s, respectively. During the second step, 100 µL of chlorobenzene was dipped onto the spinning substrate 10 s prior to the end of the program. The substrates were then annealed at 100 °C for 30 min in a dry box. The films were subsequently scratched off the glass substrates using a stainless spatula. 10 glass substrates were used in total (35 cm^2) yielding about 1 mg of a solid perovskite which was then immediately transferred into an NMR rotor.

Results and discussion

Mechanochemistry has emerged as an easy, solvent-free method of preparing large quantities of polycrystalline hybrid lead-halide perovskites that is particularly well-suited for solid-state NMR studies.[18, 20-21] Very recently we have shown that low-temperature ^{13}C solid-state MAS NMR can be used to directly probe the atomic-level phase composition of mixed-cation perovskites.[18] Here we apply this technique to show that mixed-cation $GUA_xMA_{1-x}PbI_3$ and $GUA_xFA_{1-x}PbI_3$ systems are microscopically different from the pure $GUAPbI_3$, $MAPbI_3$ and $FAPbI_3$ phases. Figure 1 shows low-temperature ^{13}C CP MAS spectra of the mechanochemically-prepared $GUA_xMA_{1-x}PbI_3$ (x=0, 0.05, 0.07, 0.10, 0.20, 0.25, 0.40, 0.95 and 1.00) and $GUA_xFA_{1-x}PbI_3$ (x=0, 0.05, 0.10, 0.20, 1.00) phases. The pure $MAPbI_3$ phase exhibits only one peak, consistent with a single chemical environment of the MA cation.[18] Upon introduction of 5 mol% of GUA this peak shifts by 0.4 ppm. Taken with observed shift for the GUA carbons at 150.3 ppm, which is very different from the shift for pure $GUAPbI_3$, as well as the powder X-ray diffraction (pXRD) data which indicates only one three-dimensional perovskite phase, *this indicates formation of a new pure mixed-cation phase in which MA is presumably interacting with the GUA cations at the atomic level.*

At 7 mol% of GUA this peak almost completely disappears and a new peak appears, shifted by 1.6 ppm. This new peak is then common to all MA/GUA compositions up to 40 mol% of GUA. Analogous changes are visible in the carbon resonances of GUA. This shift occurring between 5-10 mol% of GUA doping may be explained by invoking nearest neighbour effects. The probability of each doping GUA being surrounded by only MA cations can be evaluated in a straightforward manner if we assume random substitution (fig. S1),[22] and it drops from about 20% to 0.2% in going from 5 to 10 mol% doping, respectively. This suggests that to accommodate nearest neighbour GUA cations a change in the lattice structure occurs, as sensed by the MA and GUA shifts, owing to the increased probability of there being bulky GUA cations on two neighbouring lattice positions. This is also consistent with the pXRD data which for 5 mol% of GUA shows only a small shift of 0.02° with respect to the main reflection of pure $MAPbI_3$ at 2θ=14.2°, while for 7 mol% of GUA the peak shifts by 0.12° and becomes significantly broader, indicating a less crystalline order as compared to the parent $MAPbI_3$ lattice, as seen by pXRD, while retaining its well-defined 3D perovskite character, as evidenced by the narrow lines in the NMR spectra.

At 40 mol% of GUA, the mixed-cation phase is still present, with a broad shoulder in the MA region of the spectrum indicating a new chemical environment, distinct from that of either pure $MAPbI_3$ or the MA/GUA mixed-cation phase. pXRD indicates that compositions with x>40 mol% of GUA contain a phase-separated 1D $GUAPbI_3$-like structure whose main reflection is slightly shifted (~0.1°) with respect to pure $GUAPbI_3$ (fig. S3), which when taken with the NMR result suggests it might correspond to a 1D $GUAPbI_3$ structure in which some GUA has been replaced by MA. This hypothesis is further supported by the fact that a similarly broad MA signal is present in $GUA_{0.95}MA_{0.05}PbI_3$ (fig. 1). At 95 mol% the GUA resonances match that of pure $GUAPbI_3$, though being markedly broader than that of pure canonical $GUAPbI_3$, suggesting again that there is a mixed-cation GUA/MA 1D phase present at these high GUA loadings. Notably, very recently, Soe et al. have reported layered 2D $(GUA)(MA)_nPb_nI_{3n+1}$ (n=1-3) structures with alternating GUA and MA cations.[23]

We have also investigated thin films of $GUA_{0.05}MA_{0.95}PbI_3$ and $GUA_{0.25}MA_{0.75}PbI_3$, prepared from solution by spin coating and found that their ^{13}C CP spectra are essentially the same as those of the bulk materials made by mechanochemical synthesis (fig. S8 and S9).

We also report here the first examples of black GUA/FA mixed-cation mechanoperovskites. As shown in Figure 1c, pure $GUAPbI_3$ and α-$FAPbI_3$ yield distinct carbon signals separated by about 2 ppm. Incorporation of 5-10mol % of GUA into the α-$FAPbI_3$ lattice leads to a GUA signal which is significantly shifted and sharper than that of the pure $GUAPbI_3$ phase, accompanied by a very slight change in the shape and position of the FA peak. At 20 mol% GUA, the FA peak abruptly shifts by 1.3 ppm, indicating a change of the lattice structure. The corresponding pXRD patterns (fig. S4) indicate that the incorporation of GUA is accompanied by gradual loss of crystalline order of the parent $FAPbI_3$ perovskite, with no phase separation of either pure $GUAPbI_3$ or δ-$FAPbI_3$. The ^{13}C CP spectra thus indicate that GUA/FA form distinct pure mixed-cation phases. We find, however, that the GUA/FA phases studied here are thermodynamically unstable and become yellow within hours after annealing at 140 °C. In particular, spin-coated thin films of $GUA_xFA_{1-x}PbI_3$ are red for x=0.05, 0.10, and yellow for x=0.20, preventing direct use of these compositions as efficient light harvesters for solar cell applications. In contrast, $GUA_xMA_{1-x}PbI_3$ materials are thermodynamically stable and yield reproducible spectra several months after synthesis, if stored in a dry place.

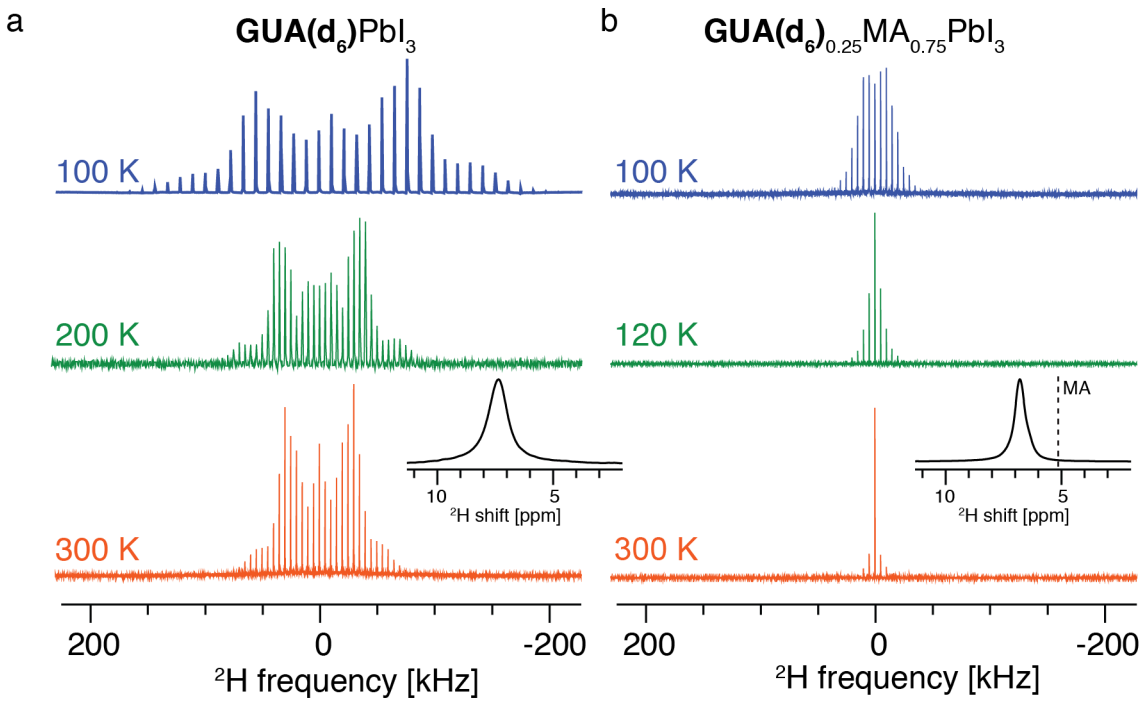

Figure 2. Variable-temperature ^{2}H echo-detected NMR spectra of (a) GUA(d$_6$)PbI$_3$, and (b) GUA(d$_6$)$_{0.25}$MA$_{0.75}$PbI$_3$ at 11.7 T and 5 kHz MAS. The spectrum at 100 K in (a) was obtained at 10 kHz MAS in a pulse-acquire experiment. The insets show a close-up of the central peak from a spectrum acquired at 20 kHz MAS. The dashed line indicates the expected position of the ND_3^+ group of MA, had it been cross-deuterated.

If GUA is incorporated on an A site into the cubo-octahedral volume of the 3D perovskite lattice, it should undergo rapid reorientation, as is the case for MA in MAPbI$_3$[18, 24-26] and FA in FAPbI$_3$ and mixed MA/FA systems[18]. Deuterium solid-state NMR is a well-established technique of probing dynamics in solids and we use it here to show that GUA is indeed rapidly reorienting in a mixed GUA/MA material, in which GUA was selectively deuterated. In ^{2}H NMR, molecular motion at a rate faster than 10^4 s^{-1} will cause averaging of the electric field gradient (EFG) tensor of the deuteron, leading to narrowing of the spectral envelope.[27] Figure 2a shows ^{2}H MAS NMR spectra of GUA(d$_6$)PbI$_3$ acquired at three temperatures between 100 and 300 K. At 100 K, the spectrum is a classic spin-1 quadrupolar pattern, exhibiting negligible motional averaging and characterized by a quadrupolar coupling constant C_Q of around 250 kHz (extracted from the spectrum through a fitting procedure). As the temperature is raised, a C_2 rotation of the –NH$_2$ groups is activated, leading to substantial narrowing of the spectrum and an apparent C_Q of around 115 kHz. No other significant changes are observed up to 300 K, consistent with the absence of whole-body reorientation of GUA(d$_6$) in GUA(d$_6$)PbI$_3$. In contrast, the 100 K spectrum of GUA(d$_6$)$_{0.25}$MA$_{0.75}$PbI$_3$ is already substantially narrowed, resembling deuterium patterns obtained for N-deuterated MA and FA in the mixed-cation MA/FA material.[18] Above 100 K the spectrum becomes narrower and nearly collapses into a single line at 300 K, indicating fast (at a rate higher than 10^6 s^{-1}), almost isotropic reorientation of the –ND$_2$ groups of GUA in this material, consistent with whole-body reorientation of the cation. In this experiment, complication might arise from the possibility of cross-deuteration between GUA(d$_6$) and MA. However, the high-resolution ^{2}H spectrum acquired at 20 kHz MAS (fig. 2b, inset), where resolution is sufficient to distinguish GUA and MA resonances shows that all deuterium in the sample belongs to GUA(d$_6$) (see fig. S12 for the assignments). *The ^{2}H NMR analysis thus proves that GUA is incorporated into the 3D perovskite structure of the parent MAPbI$_3$ material, and that it undergoes fast whole-body reorientation.*

In order to determine the reorientation rate of GUA we carried out ^{14}N solid-state NMR of the material. We have recently shown that the ^{14}N spectral envelope of a cation reorienting in the fast motion limit (FML) is indicative of the symmetry of the space in which the reorientation takes place, with lower symmetry leading to broader spectral envelopes.[18] Figures 3a and 3b show the effect of introducing GUA into the native MAPbI$_3$ and α-FAPbI$_3$ lattices, respectively. In the case of GUA$_{0.25}$MA$_{0.75}$PbI$_3$ the breadth of the methylammonium ^{14}N pattern does not visibly change with respect to pure MAPbI$_3$, indicating that there is no significant lowering of the MA reorientation symmetry. However, its shape becomes smoother, consistent with the formation of a distribution of ^{14}N sites (also reflected in the line shape of the corresponding ^{13}C resonance, which is slightly skewed towards lower shifts).[18] The change is more pronounced in GUA$_{0.25}$FA$_{0.75}$PbI$_3$ where the incorporation of GUA leads to a spectral envelope of formamidinium over 4 times broader than that of pure α-FAPbI$_3$, indicating that the symmetry of the cubo-octahedral volume in which the FA cations are reorienting has been lowered upon the incorporation of GUA.

Figure 3c shows a close-up of the ^{14}N pattern of GUA in GUA$_{0.25}$MA$_{0.75}$PbI$_3$ (top) and the fitted spectrum (center). We use this spectrum to extract quantitative rates for GUA reorientation. We have previously shown that this can be done using the diffusion-on-a-cone analysis[28], in which the motion of the cation is approximated using only two parameters: a cone semi-angle θ and a rate k.[18] The full procedure along with error estimation has been described previously.[18] The model requires the static EFG tensor of the cation (i.e. with no motional averaging), and to that end we carried out fully-relativistic DFT calculations

of guanidinium ^{14}N EFG tensors placed inside a perovskite lattice formed by $[PbI_6]^-$ octahedra, as described in the SI. Using cubic and tetragonal lattice arrangements led to results differing by less than 0.5% and we found an average predicted C_Q=3.975 MHz. Applying the diffusion-on-a-cone model (details in the SI) to reproduce the spectral envelope and line widths of the experimental spectrum (fig. 3c, bottom) yielded a reorientation rate of (18 ± 8) ps for GUA in $GUA_{0.25}MA_{0.75}PbI_3$. Importantly, the line widths of GUA seem to be limited by inhomogeneous broadening (distribution of sites) rather than by the cation reorientation, since the signal is not perfectly Lorentzian. The reported value is thus the upper bound of the reorientation rate. This result should be compared with the values we previously obtained for MA and FA in $MAPbI_3$, α-$FAPbI_3$ and $FA_{0.67}MA_{0.33}PbI_3$ (Table 1) using the same approach.[18] The reorientation rate of GUA in the material studied here is, to within error, the same or higher than that of FA in $FA_{0.67}MA_{0.33}PbI_3$. Further, the reorientation rate of MA is comparable to that of MA in the pure phase and in the mixed MA/FA phase, suggesting that the reorientation rate of a cation is largely phase independent (within the 3D perovskite family where reorientation occurs inside a cubooctahedral cavity). Very recently, Fabini *et al*. have used ^{1}H spin-lattice relaxation to probe cation dynamics in α-$FAPbI_3$.[29] We note, however, that ^{1}H relaxation, similarly to ^{2}H relaxation, results both from proton C_2-jumps (-NH_2 protons in FA), or C_3-jumps (–NH_3 and –CH_3 protons in MA) around the C-N bond, *and* from the overall cation reorientation. This convolution leads to a number of nonlinear phenomena[24, 30] and makes it difficult to quantify cation reorientation in a straightforward manner, which is why we favour the ^{14}N method used here, where the line broadening of the ^{14}N resonances is only sensitive to reorientation of the C-N bond.[18, 24]

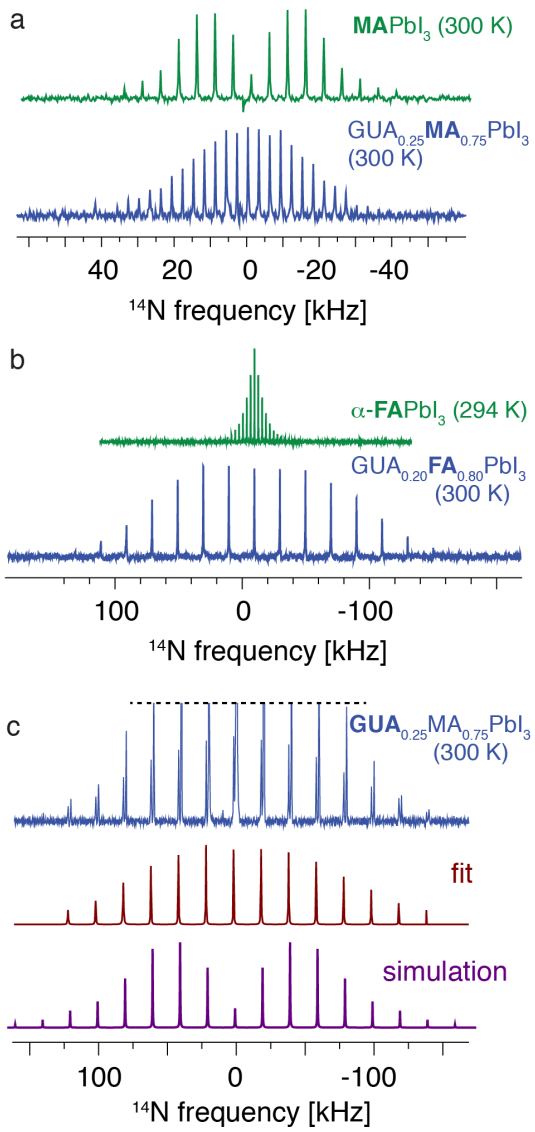

Figure 3. Room-temperature echo-detected ^{14}N MAS NMR spectra of (a) $MAPbI_3$ (top) and $GUA_{0.25}MA_{0.75}PbI_3$ (bottom, with only the MA signal visible), (b) $FAPbI_3$ (top) and $GUA_{0.20}FA_{0.80}PbI_3$ (bottom, with only the FA signal visible), (c) $GUA_{0.25}MA_{0.75}PbI_3$ (top: intensity scaled to emphasize the GUA signal, center: fit, lower: EXPRESS simulation) at 11.7 T and 5 (a, top), 3 (a, bottom; b, top), and 20 (b, bottom; c, top) kHz MAS.

Table 1. Cation reorientation rates τ from ^{14}N MAS spectra of $APbI_3$ perovskites.

A	T [K]	τ [ps]	Reference
MA	300	108 ± 18	[18]
α-FA	294	8.7 ± 0.5	[18]
$FA_{0.67}MA_{0.33}$	299	MA: 133 ± 46 FA: 12 ± 5	[18] [18]
$GUA_{0.25}MA_{0.75}$	300	MA: 113 ± 25 GUA: ≤18 ± 8	current work

By analogy with the MA/FA material we expected that the fast reorientation of GUA could stabilise the charge carrier lifetimes through the electron-rotor interaction.[19] In order to verify this hypothesis we fabricated thin films of $GUA_{0.05}MA_{0.95}PbI_3$, $GUA_{0.10}MA_{0.90}PbI_3$, $GUA_{0.25}MA_{0.75}PbI_3$, as well as $MAPbI_3$ as a reference. Figure 4a shows time-resolved photoluminescence (TRPL) spectra measured using time-correlated single photon counting (TCSPC) of the four materials. TRPL is a well-established method for characterising charge carrier lifetimes in the field of perovskite solar cells.[2, 13] We have found decay time constants of (81 ± 2) ns, (0.935 ± 0.03) µs, (3.1 ± 0.4) µs and (0.369 ± 0.004) µs for $MAPbI_3$, $GUA_{0.05}MA_{0.95}PbI_3$, $GUA_{0.10}MA_{0.90}PbI_3$ and $GUA_{0.25}MA_{0.75}PbI_3$, respectively. *This spectacular increase of charge carrier lifetimes, by 2 orders of magnitude, upon guanidinium incorporation is in line with the effect of electron-rotor interaction[19] since GUA reorients an order of magnitude faster than MA in the mixed-cation material (Table 1).* Moreover, the photoluminescence intensity measured on thin films of $GUA_{0.05}MA_{0.95}PbI_3$, $GUA_{0.10}MA_{0.90}PbI_3$, and $GUA_{0.25}MA_{0.75}PbI_3$ is significantly higher than that of $MAPbI_3$ (fig. S7) and the three materials exhibit a similar band gap (fig. S6), consistent with the results previously reported by Yang.[13]

Further, in order to confirm the expected beneficial effect of such long charge carrier lifetimes on photovoltaic performance, we fabricated solar cell devices using $GUA_{0.05}MA_{0.95}PbI_3$, $GUA_{0.10}MA_{0.90}PbI_3$ as well as $MAPbI_3$ as a reference. Figure 4b shows their PV metrics measured on four devices for each composition. Incorporation of 5 mol% GUA leads to an increase in V_{OC} of over 50 mV with respect to the reference $MAPbI_3$ material. This in turn produces a substantial gain in the PCE from 18.5 to over 19.0 % for the best performing samples. However, incorporation of more than 5 mol% GUA reduces the PCE due to a decrease in the fill factor FF and the short circuit photocurrent indicating that higher guanidinium levels affect adversely the transport and collection of photogenerated charge carriers.

Since the PV metrics deteriorated rapidly above 5 mol% GUA incorporation, we only tested PV in compositions up to 10 mol% GUA. Given that phase separation occurs for compositions with more than about 40 mol% GUA, in the ^{14}N MAS NMR experiment we studied an intermediate composition with 25 mol% GUA to ensure good sensitivity. We do not expect the reorientation rate of GUA to change significantly between 5 and 25 mol% since the cation reorients in a cubooctahedral cavity of similar volume (for example, the reduced lattice parameter ratio, $c/\sqrt{2}a$, changes from 1.010 to 1.000 on going from tetragonal (298 K) to cubic (327 K) $MAPbI_3$)[31]. We expect a change of a similar order of magnitude here, upon GUA incorporation into the tetragonal $MAPbI_3$ phase. One can expect, however, that for these high GUA/MA ratios, the lattice experiences additional strain due to the presence of a large number of bulky GUA cations. Beyond the stabilization effect provided by fast GUA dynamics, it cannot be excluded that this additional strain adversely affects charge carrier stability. Further studies are underway to explore the root cause of this behaviour.

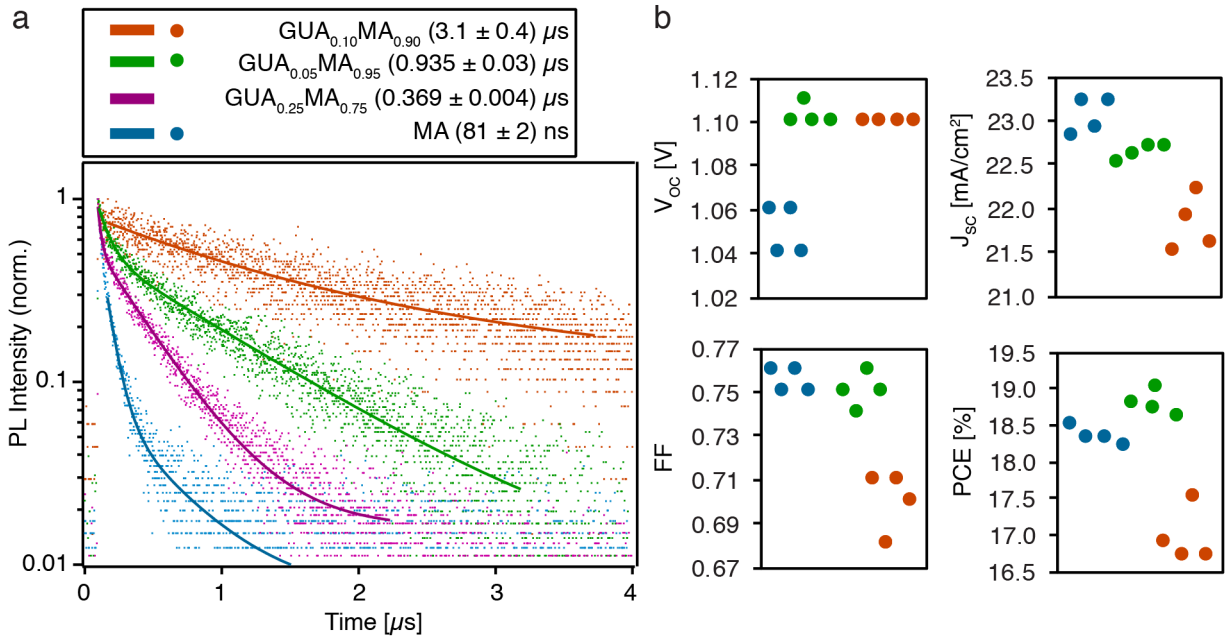

Figure 4. (a) Time-resolved photoluminescence (TRPL) measured using time-correlated single photon counting (TCSPC) of $GUA_xMA_{1-x}PbI_3$ thin films (x=0, 0.05, 0.10 and 0.25). The data was fitted using double exponentials and the value with the higher weighting coefficient is reported in the label. The reported error is one standard deviation. (b) Photovoltaic metrics of solar cells fabricated using $GUA_xMA_{1-x}PbI_3$ (x=0, 0.05, 0.10).

In conclusion, we have shown that guanidinium is readily incorporated into parent $MAPbI_3$ and α-$FAPbI_3$ perovskite lattices. $GUA_xMA_{1-x}PbI_3$ compositions are stable for x < 40 mol% for at least months, and we have shown that in $GUA_{0.25}MA_{0.75}PbI_3$ guanidinium undergoes rapid reorientation on the picosecond timescale. This leads to unprecedentedly long charge carrier lifetimes in guanidinium-doped $GUA_xMA_{1-x}PbI_3$ perovskite materials, as measured by time-resolved photoluminescence, and in turn to improved photovoltaic performance. On the other hand, although black mixed-cation $GUA_xFA_{1-x}PbI_3$ phases do form, they are thermodynamically unstable and become yellow within hours from annealing, which indicates that guanidinium alone does not sufficiently stabilise the α-$FAPbI_3$ perovskite structure.

Associated Content

Supporting Information

Supplementary information (details of mechanosynthesis, pXRD, details of DFT calculations, NMR, UV-VIS, PL and TRPL experiments, details of PV device fabrication) is available in the online version of the paper. Requests for additional data and correspondence should be addressed to M.G or L.E.

Author Information

Corresponding Authors

*lyndon.emsley@epfl.ch
*michael.graetzel@epfl.ch
*lewin@ch.pw.edu.pl

Notes

The authors declare no competing financial interest.

Acknowledgement

We thank Im Jeong-Hyeok for preparing thin films of $GUA_xFA_{1-x}PbI_3$ materials. This work was supported by ERC Advanced Grant No. 320860 and Swiss National Science Foundation Grant No. 200021_160112. D. P. acknowledges support from the Marie Skłodowska-Curie fellowship, H2020, grant agreement no. 707168. J. L., M. S. and M. G acknowledge funding from the EU Horizon 2020 programme, through the FET Open Research and Innovation Action, grant agreement no. 687008. M. G. and S.M.Z thank the King Abdulaziz City for Science and Technology (KACST) and the SNSF for a joint research project (IZLRZ2_164061) under Scientific & Technological Cooperation Programme Switzerland-Russia.

References

1. Jeon, N. J.; Noh, J. H.; Yang, W. S.; Kim, Y. C.; Ryu, S.; Seo, J.; Seok, S. I., *Nature* **2015,** *517*, 476-480.
2. Pellet, N.; Gao, P.; Gregori, G.; Yang, T. Y.; Nazeeruddin, M. K.; Maier, J.; Gratzel, M., *Angew. Chem. Int. Ed.* **2014,** *53*, 3151-3157.
3. Li, X.; Bi, D. Q.; Yi, C. Y.; Decoppet, J. D.; Luo, J. S.; Zakeeruddin, S. M.; Hagfeldt, A.; Gratzel, M., *Science* **2016,** *353*, 58-62.
4. Duong, T.; Mulmudi, H. K.; Shen, H. P.; Wu, Y. L.; Barugkin, C.; Mayon, Y. O.; Nguyen, H. T.; Macdonald, D.; Peng, J.; Lockrey, M.; Li, W.; Cheng, Y. B.; White, T. P.; Weber, K.; Catchpole, K., *Nano Energy* **2016,** *30*, 330-340.
5. Lee, J. W.; Kim, D. H.; Kim, H. S.; Seo, S. W.; Cho, S. M.; Park, N. G., *Adv. Energ. Mater.* **2015,** *5*, 1501310-1501318.
6. Xia, X.; Wu, W. Y.; Li, H. C.; Zheng, B.; Xue, Y. B.; Xu, J.; Zhang, D. W.; Gao, C. X.; Liu, X. Z., *Rsc Advances* **2016,** *6*, 14792-14798.
7. Yi, C. Y.; Luo, J. S.; Meloni, S.; Boziki, A.; Ashari-Astani, N.; Gratzel, C.; Zakeeruddin, S. M.; Rothlisberger, U.; Gratzel, M., *Energy Environ. Sci.* **2016,** *9*, 656-662.
8. Park, Y. H.; Jeong, I.; Bae, S.; Son, H. J.; Lee, P.; Lee, J.; Lee, C. H.; Ko, M. J., *Adv. Funct. Mater.* **2017,** *27*, 1605988-16059815.
9. Saliba, M.; Matsui, T.; Seo, J. Y.; Domanski, K.; Correa-Baena, J. P.; Nazeeruddin, M. K.; Zakeeruddin, S. M.; Tress, W.; Abate, A.; Hagfeldt, A.; Gratzel, M., *Energy Environ. Sci.* **2016,** *9*, 1989-1997.
10. Zhang, M.; Yun, J. S.; Ma, Q. S.; Zheng, J. H.; Lau, C. F. J.; Deng, X. F.; Kim, J.; Kim, D.; Seidel, J.; Green, M. A.; Huang, S. J.; Ho-Baillie, A. W. Y., *ACS Energy Lett.* **2017,** *2*, 438-444.

11. Stranks, S. D.; Snaith, H. J., *Nat. Nano.* **2015,** *10*, 391-402.
12. Giorgi, G.; Fujisawa, J. I.; Segawa, H.; Yamashita, K., *J. Phys. Chem. C* **2015,** *119*, 4694-4701.
13. De Marco, N.; Zhou, H. P.; Chen, Q.; Sun, P. Y.; Liu, Z. H.; Meng, L.; Yao, E. P.; Liu, Y. S.; Schiffer, A.; Yang, Y., *Nano Lett.* **2016,** *16*, 1009-1016.
14. Hou, X. M.; Hu, Y.; Liu, H. W.; Mei, A. Y.; Li, X.; Duan, M.; Zhang, G. A.; Rong, Y. G.; Han, H. W., *J. Mater. Chem. A* **2017,** *5*, 73-78.
15. Jodlowski, A. D.; Yepez, A.; Luque, R.; Camacho, L.; de Miguel, G., *Angew. Chem. Intern. Ed.* **2016,** *55*, 14972-14977.
16. Zhu, X. Y.; Podzorov, V., *J. Phys. Chem. Lett.* **2015,** *6*, 4758-4761.
17. Neukirch, A. J.; Nie, W. Y.; Blancon, J. C.; Appavoo, K.; Tsai, H.; Sfeir, M. Y.; Katan, C.; Pedesseau, L.; Even, J.; Crochet, J. J.; Gupta, G.; Mohite, A. D.; Tretiak, S., *Nano Lett.* **2016,** *16*, 3809-3816.
18. Kubicki, D.; Prochowicz, D.; Hofstetter, A.; Pechy, P.; Zakeeruddin, S. M.; Graetzel, M.; Emsley, L., *J. Am. Chem. Soc.* **2017,** *139*, 10055-10061.
19. Gong, J.; Yang, M. J.; Ma, X. C.; Schaller, R. D.; Liu, G.; Kong, L. P.; Yang, Y.; Beard, M. C.; Lesslie, M.; Dai, Y.; Huang, B. B.; Zhu, K.; Xu, T., *J. Phys. Chem. Lett.* **2016,** *7*, 2879-2887.
20. Prochowicz, D.; Franckevicius, M.; Cieslak, A. M.; Zakeeruddin, S. M.; Gratzel, M.; Lewinski, J., *J. Mater. Chem. A* **2015,** *3*, 20772-20777.
21. Prochowicz, D.; Yadav, P.; Saliba, M.; Saski, M.; Zakeeruddin, S. M.; Lewinski, J.; Graetzel, M., *ACS Appl. Mat. Inter.* **2017,** *9*, 28418-28425.
22. Faulkner, J. S.; Pella, S.; Rusanu, A.; Puzyrev, Y., *Short-range order parameters in FCC binary alloys*. Springer, Boston, MA: Boston, MA, 2005; p 145-158.
23. Myae Myae Soe, C.; Stoumpos, C. C.; Kepenekian, M.; Traoré, B.; Tsai, H.; Nie, W.; Wang, B.; Katan, C.; Seshadri, R.; Mohite, A. D.; Even, J.; Marks, T. J.; Kanatzidis, M. G., *J. Am. Chem. Soc.* **2017,** *139*, 16297-16309.
24. Knop, O.; Wasylishen, R. E.; White, M. A.; Cameron, T. S.; Vanoort, M. J. M., *Can. J. Chem.* **1990,** *68*, 412-422.
25. Roiland, C.; Trippe-Allard, G.; Jemli, K.; Alonso, B.; Ameline, J. C.; Gautier, R.; Bataille, T.; Le Polles, L.; Deleporte, E.; Even, J.; Katan, C., *Phys. Chem. Chem. Phys.* **2016,** *18*, 27133-27142.
26. Franssen, W. M. J.; van Es, S. G. D.; Dervisoglu, R.; de Wijs, G. A.; Kentgens, A. P. M., *J. Phys. Chem. Lett.* **2017,** *8*, 61-66.
27. O'Dell, L. A.; Ratcliffe, C. I., Quadrupolar NMR to Investigate Dynamics in Solid Materials. In *NMR of Quadrupolar Nuclei in Solid Materials*, Wasylishen, R. E.; Ashbrook, S. E.; Wimperis, S., Eds. Wiley: 2011.
28. Torchia, D. A.; Szabo, A., *J. Magn. Reson.* **1982,** *49*, 107-121.
29. Fabini, D. H.; Siaw, T. A.; Stoumpos, C. C.; Laurita, G.; Olds, D.; Page, K.; Hu, J. G.; Kanatzidis, M. G.; Han, S.; Seshadri, R., *J. Am. Chem. Soc.* **2016**, 10.1021/jacs.7b09536.
30. Aronson, M.; Beckmann, P.; Guerra, V.; Schwamb, C.; Tan, S. L., *Mol. Phys.* **1980,** *41*, 1239-1258.
31. Weller, M. T.; Weber, O. J.; Henry, P. F.; Di Pumpo, A. M.; Hansen, T. C., *Chem. Commun.* **2015,** *51*, 4180-4183.

TOC:

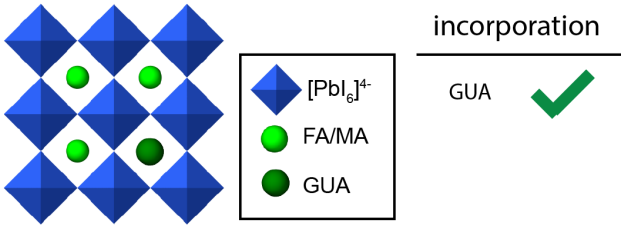

Formation of stable mixed guanidinium-methylammonium phases with exceptionally long carrier lifetimes for high efficiency lead iodide-based perovskite photovoltaics

Dominik J. Kubicki,[a] Daniel Prochowicz,[b,c] Albert Hofstetter,[a] Marcin Saski,[c] Pankaj Yadav,[b] Dongqin Bi,[b] Norman Pellet,[b] Janusz Lewiński,*[c] Shaik M. Zakeeruddin,[b] Michael Grätzel,*[b] Lyndon Emsley*[a]

[a]*Laboratory of Magnetic Resonance, Institute of Chemical Sciences and Engineering, Ecole Polytechnique Fédérale de Lausanne (EPFL), CH-1015 Lausanne, Switzerland*
[b]*Laboratory of Photonics and Interfaces, Institute of Chemical Sciences and Engineering, Ecole Polytechnique Fédérale de Lausanne (EPFL), CH-1015 Lausanne, Switzerland*
[c]*Institute of Physical Chemistry, Polish Academy of Sciences, Kasprzaka 44/52, 01-224 Warsaw, Poland.*

[d]*School of Technology, Pandit Deendayal Petroleum University, Gandhinagar 382 007, Gujarat*

Table of Contents

The Goldschmidt tolerance factor analysis of MA/GUA and FA/GUA mixed-cation lead iodides

The possibility of formation of mixed-cation MA/GUA and FA/GUA 3D perovskite phases was estimated using the Goldschmidt tolerance factor $t = \frac{R_A + R_X}{\sqrt{2}(R_B + R_X)}$, where R_A, R_B and R_X are the effective ionic radii in a ABX_3 perovskite lattice. A perovskite structure is likely to form when $0.8 < t < 1.0$. The following values were used in the calculations: I^- 220 pm (R_X), Pb^{2+} 119pm (R_B), MA 217 pm, FA 253 pm and GUA 278 pm (R_A).[2] The cation radii in mixed-cation materials were calculated as a weighted average of the radii of the two cations.

Table S1. Calculated Goldschmidt tolerance factors for $GUA_xMA_{1-x}PbI_3$ and $GUA_xFA_{1-x}PbI_3$ materials (**in bold** – compositions studied by solid-state NMR in this work).

Composition	R_A [pm]	t
$MAPbI_3$	**217.00**	**0.91**
$GUA_{0.05}MA_{0.95}PbI_3$	**220.05**	**0.92**
$GUA_{0.10}MA_{0.90}PbI_3$	**223.10**	**0.92**
$GUA_{0.15}MA_{0.85}PbI_3$	226.15	0.93
$GUA_{0.20}MA_{0.80}PbI_3$	229.20	0.94
$GUA_{0.25}MA_{0.75}PbI_3$	**232.25**	**0.94**
$GUA_{0.30}MA_{0.70}PbI_3$	235.30	0.95
$GUA_{0.35}MA_{0.65}PbI_3$	238.35	0.96
$GUA_{0.40}MA_{0.60}PbI_3$	**241.40**	**0.96**
$GUA_{0.45}MA_{0.55}PbI_3$	244.45	0.97
$GUA_{0.50}MA_{0.50}PbI_3$	247.50	0.98
$GUA_{0.55}MA_{0.45}PbI_3$	250.55	0.98
$GUA_{0.60}MA_{0.40}PbI_3$	253.60	0.99
$GUA_{0.65}MA_{0.35}PbI_3$	256.65	0.99
$GUA_{0.70}MA_{0.30}PbI_3$	259.70	1.00
$GUA_{0.75}MA_{0.25}PbI_3$	262.75	1.01
$GUA_{0.80}MA_{0.20}PbI_3$	265.80	1.01
$GUA_{0.85}MA_{0.15}PbI_3$	268.85	1.02
$GUA_{0.90}MA_{0.10}PbI_3$	271.90	1.03
$GUA_{0.95}MA_{0.05}PbI_3$	**274.95**	**1.03**
$GUAPbI_3$	**278.00**	**1.04**

Table 2. continued

Composition	R_A [pm]	t
$FAPbI_3$	**253.00**	**0.99**
$GUA_{0.05}FA_{0.95}PbI_3$	**254.25**	**0.99**
$GUA_{0.10}FA_{0.90}PbI_3$	**255.50**	**0.99**
$GUA_{0.15}FA_{0.85}PbI_3$	256.75	0.99
$GUA_{0.20}FA_{0.80}PbI_3$	**258.00**	**1.00**
$GUA_{0.25}FA_{0.75}PbI_3$	259.25	1.00
$GUA_{0.30}FA_{0.70}PbI_3$	260.50	1.00
$GUA_{0.35}FA_{0.65}PbI_3$	261.75	1.00
$GUA_{0.40}FA_{0.60}PbI_3$	263.00	1.01
$GUA_{0.45}FA_{0.55}PbI_3$	264.25	1.01
$GUA_{0.50}FA_{0.50}PbI_3$	265.50	1.01
$GUA_{0.55}FA_{0.45}PbI_3$	266.75	1.02
$GUA_{0.60}FA_{0.40}PbI_3$	268.00	1.02
$GUA_{0.65}FA_{0.35}PbI_3$	269.25	1.02
$GUA_{0.70}FA_{0.30}PbI_3$	270.50	1.02
$GUA_{0.75}FA_{0.25}PbI_3$	271.75	1.03
$GUA_{0.80}FA_{0.20}PbI_3$	273.00	1.03
$GUA_{0.85}FA_{0.15}PbI_3$	274.25	1.03
$GUA_{0.90}FA_{0.10}PbI_3$	275.50	1.03
$GUA_{0.95}FA_{0.05}PbI_3$	276.75	1.04
$GUAPbI_3$	**278.00**	**1.04**

Perovskite synthesis

Starting materials were stored inside a glove box under argon. Perovskite powders were synthesized by grinding the reactants in an electric ball mill (Retsch Ball Mill MM-200, a grinding jar (10 ml) and a ball with ⌀10 mm) for 30 min at 25 Hz. The resulting perovskite powders were annealed at 140 °C for 10 minutes to reproduce the thin-film synthetic procedure.[3]

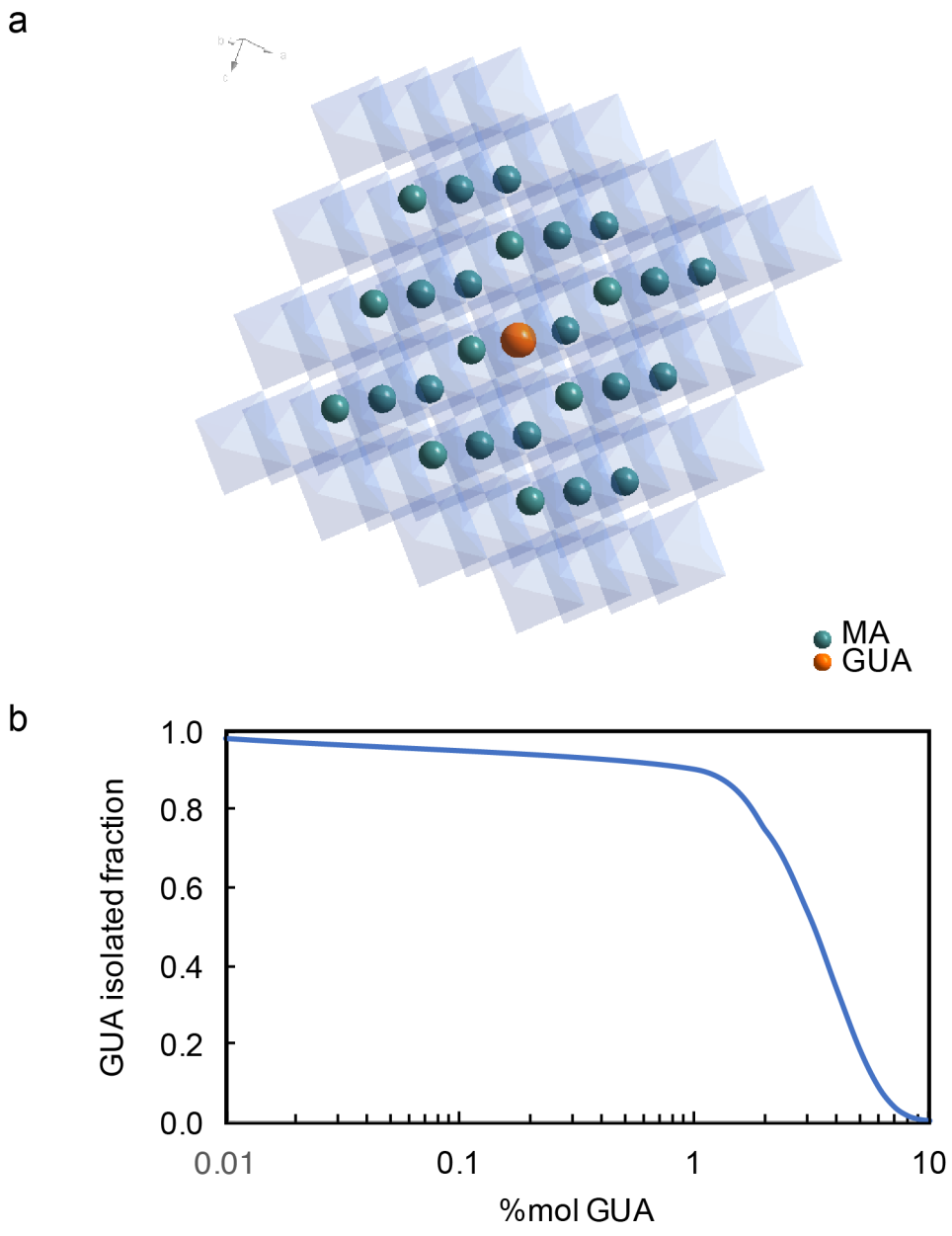

Figure S1. a) Schematic representation of neighbouring MA cations surrounding a guanidinium cation in a 3D cubic perovskite structure. (b) Fraction of GUA without GUA neighbours (isolated fraction) in a 3D perovskite lattice of $GUA_xMA_{1-x}PbI_3$ vs.

GUA doping x. The binomial distribution was calculated by assuming that each A site has 26 closest A neighbours.

Powder X-ray Diffraction

Diffractograms were recorded on an X'Pert MPD PRO (Panalytical) diffractometer equipped with a ceramic tube (Cu anode, λ = 1.54060 Å), a secondary graphite (002) monochromator and an RTMS X'Celerator (Panalytical) in an angle range of 2θ = 5° to 40°, by step scanning with a step of 0.02 degree.

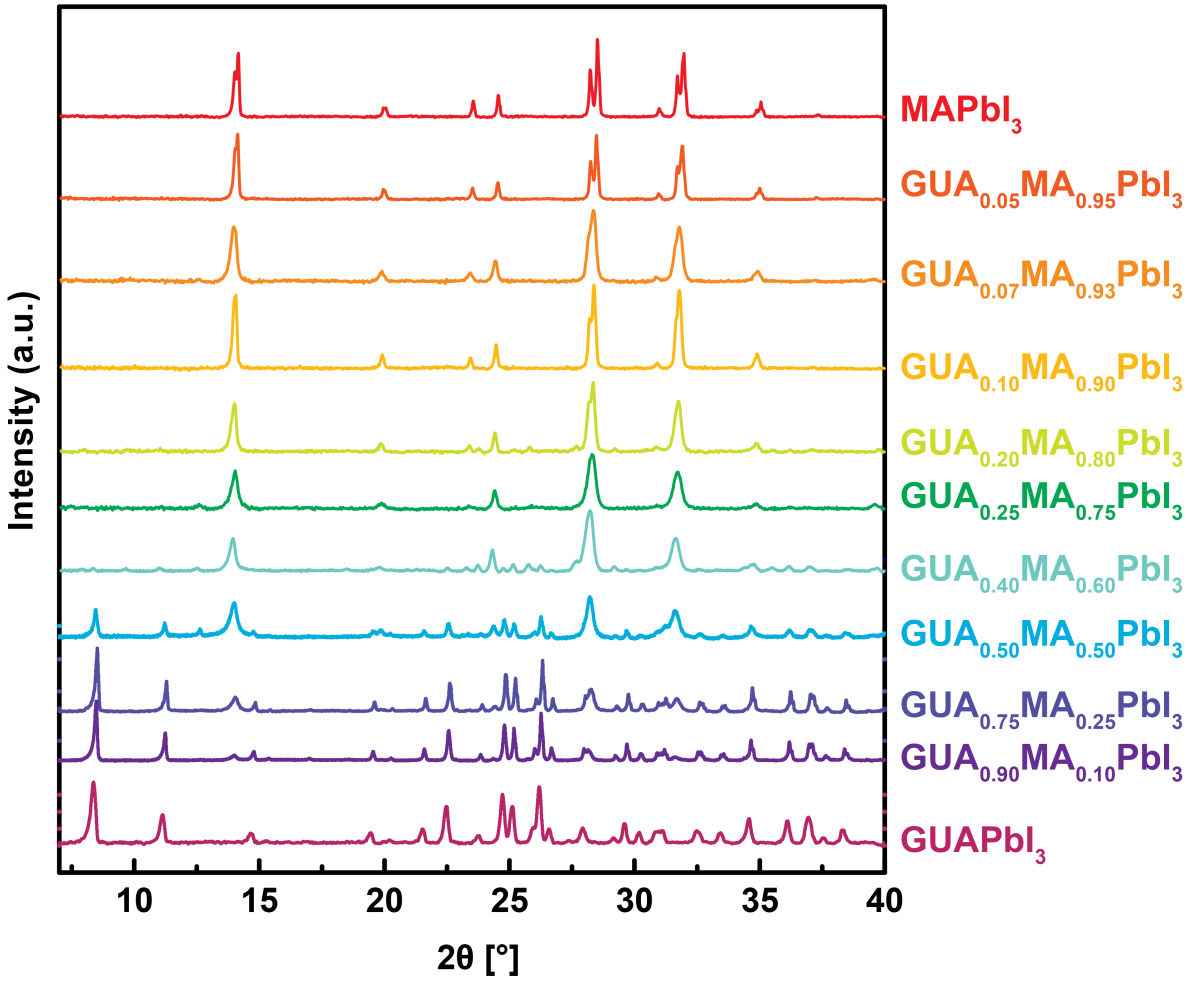

Figure S2. pXRD patterns of the $GUA_xMA_{1-x}PbI_3$ compositions.

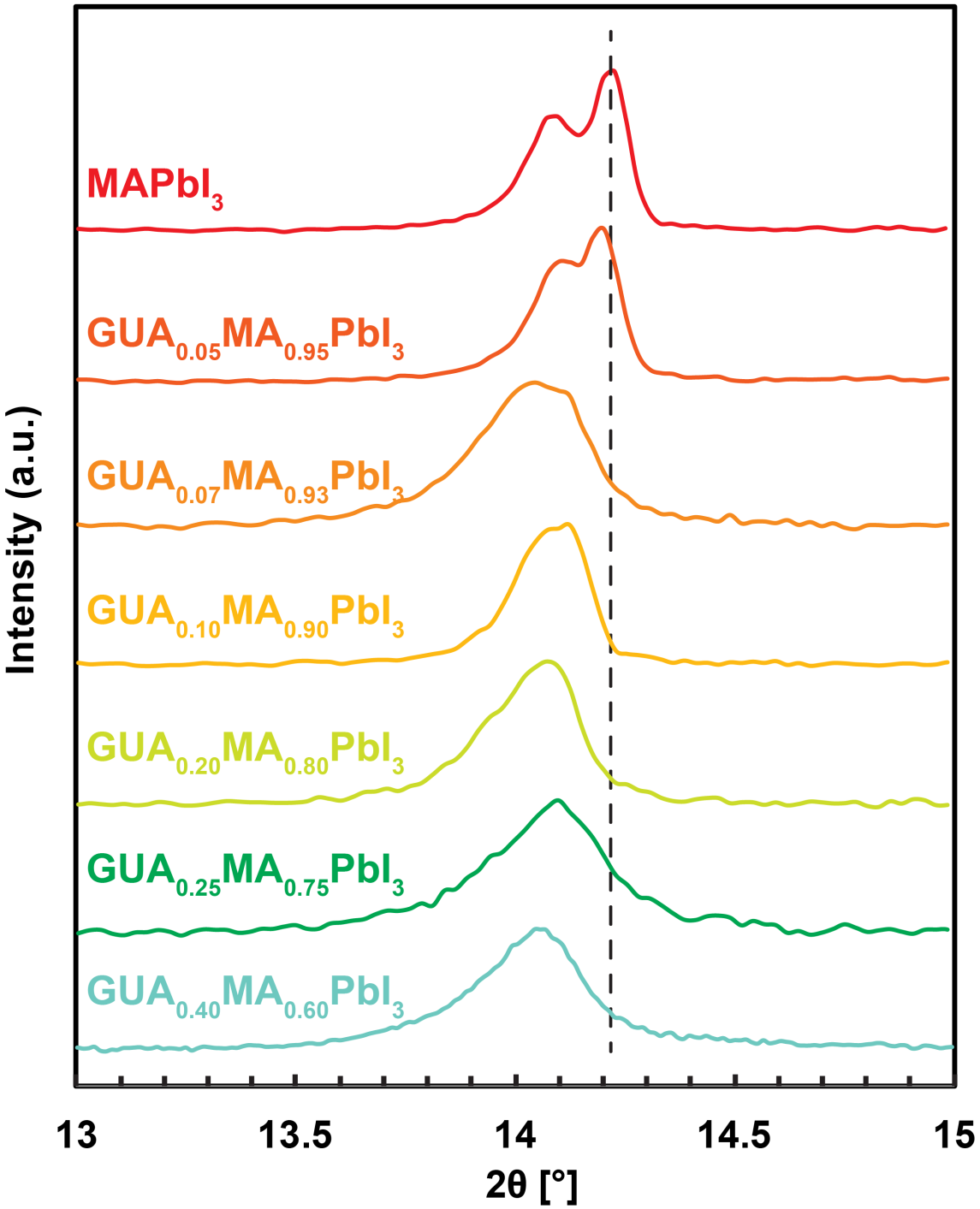

Figure S3. Close-up of the main reflexion in the pXRD patterns of $GUA_xMA_{1-x}PbI_3$ (x=0, 0.05, 0.07, 0.10, 0.20, 0.25 and 0.40).

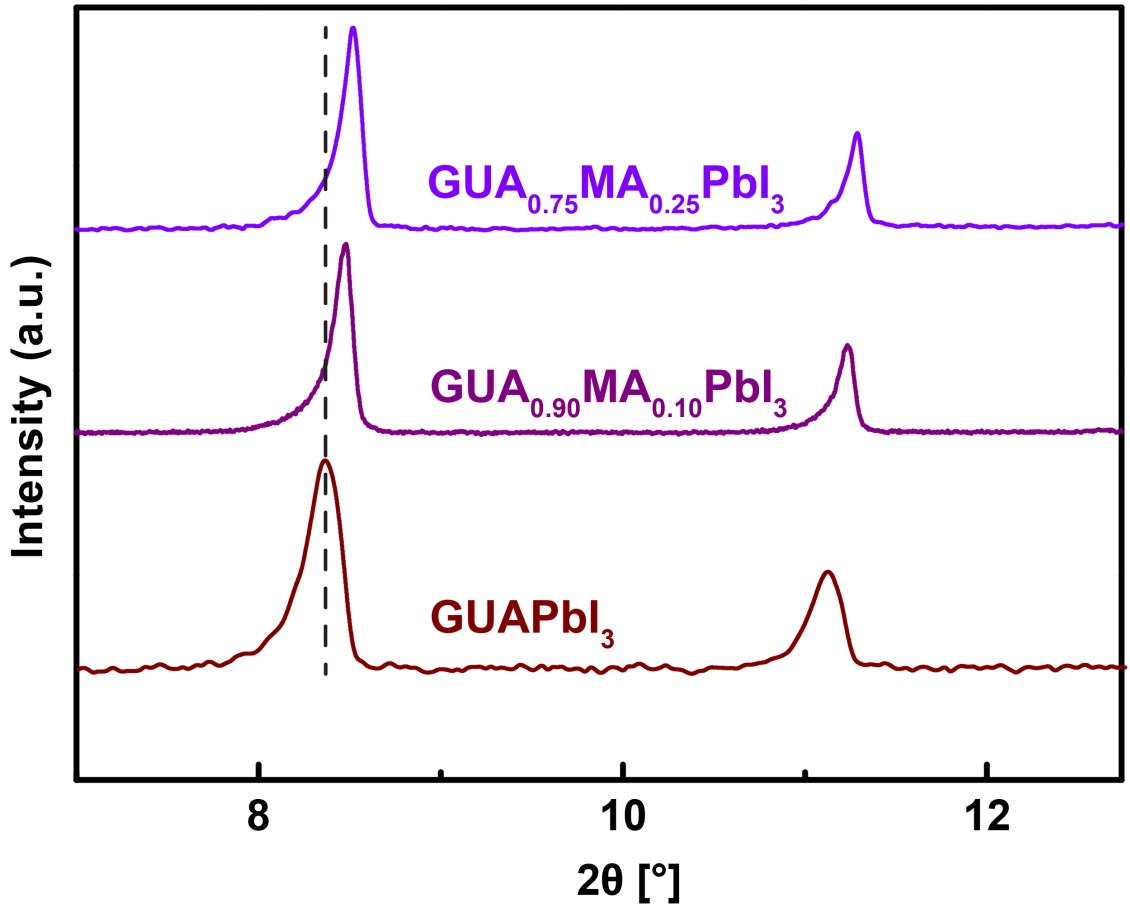

Figure S4. Close-up of the main reflexion in the pXRD patterns of $GUA_xMA_{1-x}PbI_3$ (x=0.75, 0.90 and 1.00).

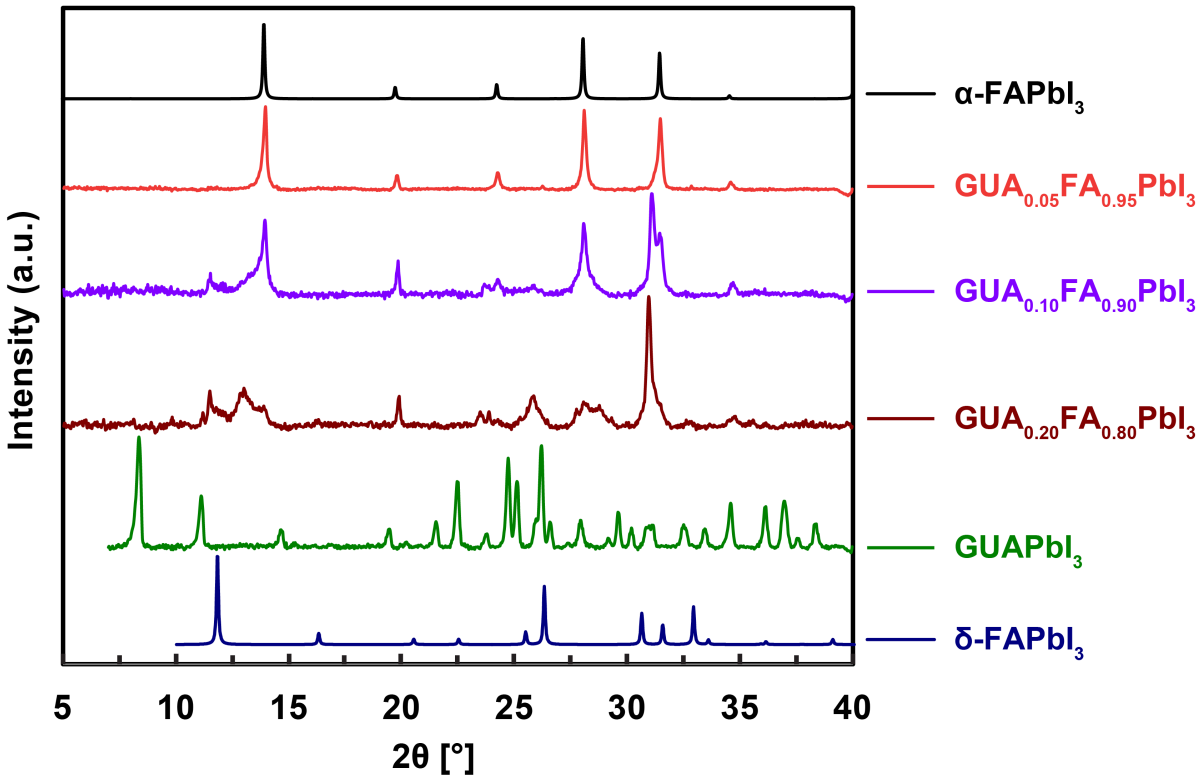

Figure S5. pXRD patterns of the $GUA_xFA_{1-x}PbI_3$ compositions.

UV-VIS measurements

UV-VIS measurements were carried out on a Varian Cary 5 spectrophotometer.

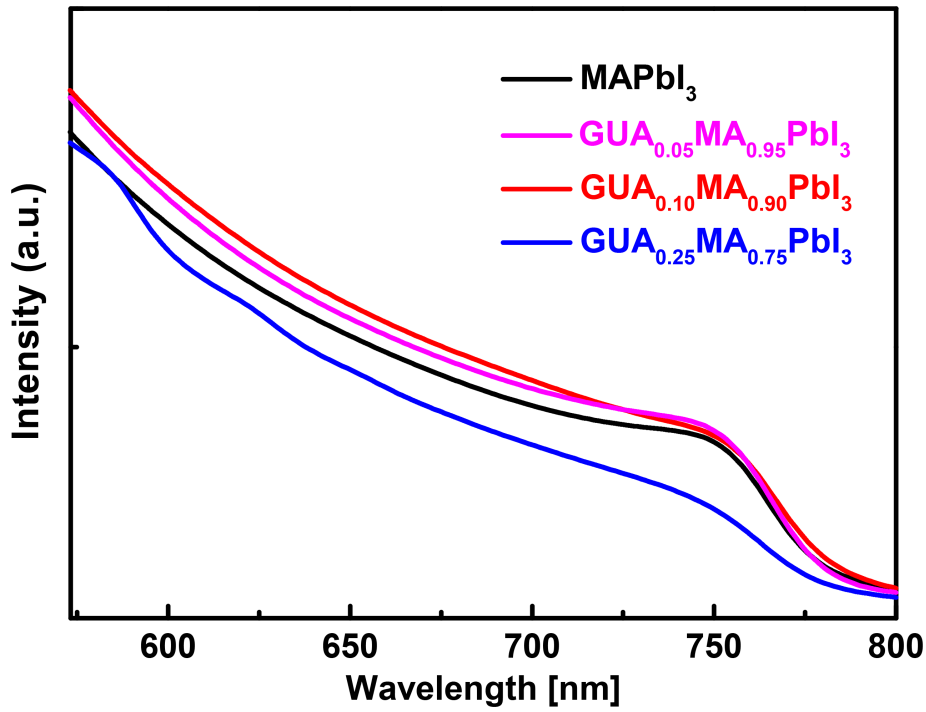

Figure S6. UV-VIS absorption spectra of $GUA_xMA_{1-x}PbI_3$ (x=0, 0.05, 0.10 and 0.25) thin films.

Photoluminescence measurements

PL measurements were carried out on a Fluorolog 322 (Horiba Jobin Ybon Ltd) spectrofluorometer with excitation at 460 nm and detection of the range between 650 and 850 nm.

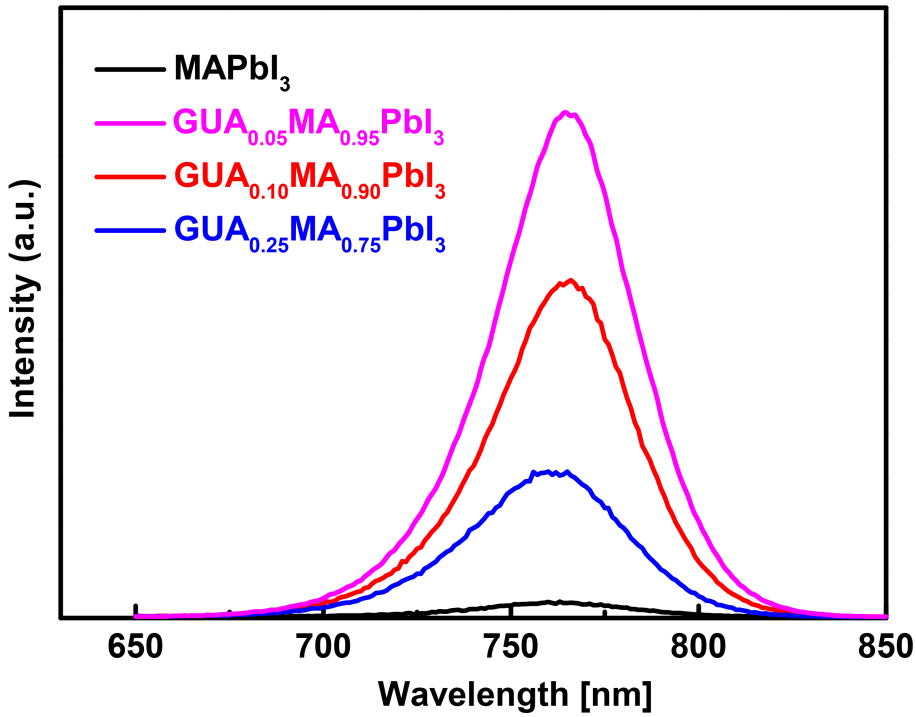

Figure S7. Photoluminescence spectra of $GUA_xMA_{1-x}PbI_3$ (x=0, 0.05, 0.10 and 0.25) thin films.

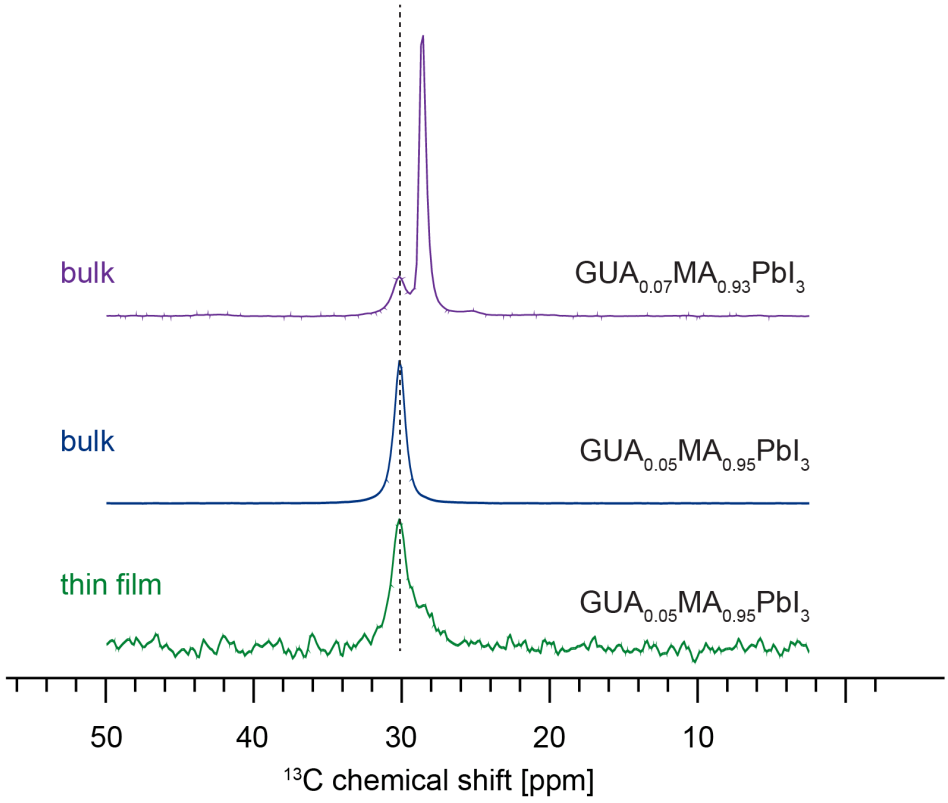

Figure S8. Low-temperature (100 ± 3 K) ^{13}C CP MAS spectra of $GUA_{0.05}MA_{0.95}PbI_3$ prepared in bulk and as a spin-coated thin film. In the latter case, sensitivity was sufficient to detect only the MA signal, hence only this part of the spectrum is shown. The spectrum of bulk $GUA_{0.07}MA_{0.93}PbI_3$ in given at the top for comparison.

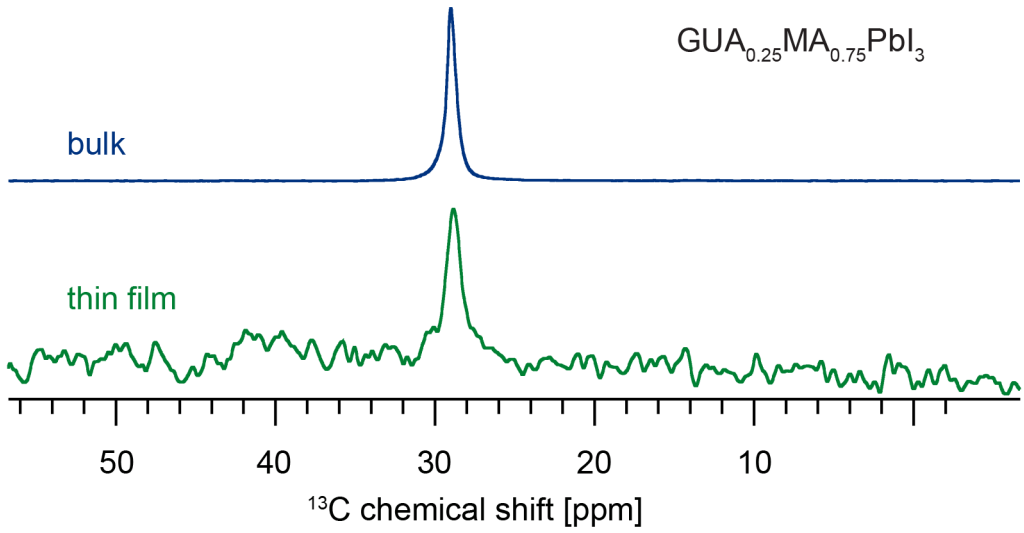

Figure S9. Low-temperature (100 ± 3 K) ^{13}C CP MAS spectra of $GUA_{0.25}MA_{0.75}PbI_3$ prepared in bulk (top) and as a spin-coated thin film (bottom). In the latter case, sensitivity was sufficient to detect only the MA signal, hence only this part of the spectrum is shown.

Table S2. Full widths at half maximum (FWHM) and standard deviations (σ) obtained by fitting (SOLA) the most intense peaks (best SNR) in ^{14}N MAS spectra of $GUA_{0.25}MA_{0.75}PbI_3$ at 300 K.

	GUA (20 kHz MAS)	MA (5 kHz MAS)
	FWHM [Hz]	FWHM [Hz]
	369	65.4
	316	67.7
	303	67.2
	277	66.6
	232	67.8
	225	65.7
	275	60.8
	261	64.7
	277	52.8
	261	65.0
	322	56.7
		66.8
		70.2
avg	**283**	**64.4**
STD	**42**	**5**

Diffusion-on-a-cone model

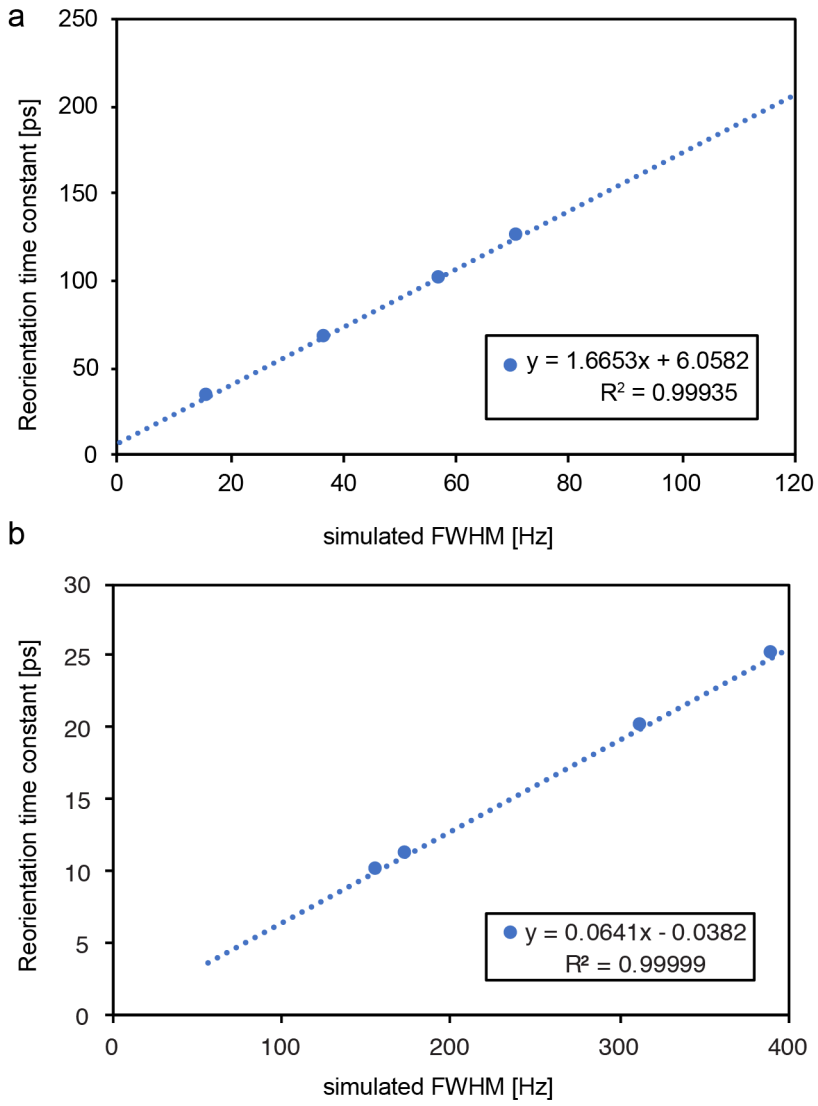

Figure S10. Diffusion-on-a-cone averaging using 10 points on a cone for (a) MA in $GUA_{0.25}MA_{0.75}PbI_3$ at 300 K (C_Q=0.771 MHz, θ=51.7°), (b) GUA in $GUA_{0.25}MA_{0.75}PbI_3$ at 300 K (C_Q= 3.975 MHz, θ=55.20°). For further details see the description in the paper by Kubicki *et al.*[1]

Time-resolved photoluminescence

Photoluminescence measurements were carried out on a Horiba Jobin Ybon Ltd. spectrofluorometer equipped with a NanoLED® laser diode with a 100 kHz repetition rate. The excitation wavelength was 406 nm. The photoluminescence signal was filtered through a cut-off filter (520 nm). The samples were mounted at 60° from the emission beam and the emission decay recorded at 90° from the incident beam path. The PL was filtered through a Bragg interference filter (cantered at 768nm) before detection.

Details of solar cell device fabrication

Devices were prepared on plasma-cleaned conductive fluorine-doped tin oxide (FTO) coated glass substrates. A compact thick titanium dioxide layer was deposited by spray pyrolysis of 9 ml ethanol solution containing 0.6 mL titanium diiso-propoxide bis(acetylacetonate) solution (75% in 2-propanol, Sigma-Aldrich) and 0.4 mL acetylacetone at 450° C in air. On top of this compact layer, a 150 nm-thick mesoporous titanium dioxide layer was prepared by spin-coating 40 nm sized mesoporous TiO_2 (anatase) nanoparticles (Cristal Ltd. UK, GP350 grade) diluted in ethanol (1:6 wt/wt) at 5000 rpm for 10 s. The films were then gradually heated to 500 °C and sintered at that temperature for 1.5 h under oxygen atmosphere.

The stock 1.45 M solutions of GUA·HI, MA·HI and PbI_2 were prepared by dissolving them in anhydrous DMSO solvent mixture by vigorous stirring at 60°C. 5 mol% excess of PbI_2 was used. The perovskite solution was spin coated in a two steps program at 1000 and 6000 rpm for 10 and 20 s respectively. During the second step, 100 µL of chlorobenzene were dripped on the spinning substrate 10 s prior to the end of the program. The substrates were then annealed at 100°C for 30 min in a nitrogen filled glove box.

Hole transporting material (HTM) solution was prepared by dissolving 74 mg spiro-MeOTAD in 1 mL chlorobenzene and additionally mixing it with 17.5 μL of lithium bis(trifluoromethylsulphonyl)imide (stock solution Li-TFSI 520 $mg \cdot mL^{-1}$ in acetonitrile), 28.8 μL tert-butylpyridine and 29 µL of tris(2-(1H-pyrazol-1-yl)-4-tert-butylpyridine)cobalt(III) bis(trifluoromethylsulphonyl) imide (stock solution FK 209, 300 mg·ml–1 in acetonitrile). Subsequently, HTM was deposited on top of the perovskite layer by spin coating at 4000 rpm for 20 s. Finally, 80 nm of gold top electrode was thermally evaporated under high vacuum. The active area of the devices is approximately 0.16 cm^2.

Device characterization. The *J-V* characteristics of the devices were measured under 100 mW/cm^2 conditions using a 450 W Xenon lamp (Oriel), as a light source, equipped with a Schott K113 Tempax sunlight filter (Praezisions Glas & Optik GmbH) to match the emission spectra to the AM1.5G standard in the region of 350-750 nm. The current–voltage characteristics of the devices were obtained by applying external potential bias to the cell while recording the generated photocurrent using a Keithley (Model 2400) digital source meter. The *J–V* curves of all devices were measured by masking the active area with a metal mask of area 0.16 cm^2.

Details of DFT calculations

Cluster generation

We start from the assumption, that GUA is incorporated into the FA/MA-PbI3 lattice, replacing the FA/MA cation, without significantly changing the perovskite lattice formed by the [PbI^6]- octahedra. Thus, in a first step we replace the FA/MA ions of the $FAPbI_3$[4] and tetragonal (black) $MAPbI_3$[5] crystal structures by GUA cations. Next, we optimize the positions of the light atoms (^{13}C, ^{15}N and ^{1}H) inside the [$PbI_{6]4-}$ cage using a periodic system within the density functional theory (DFT) framework and the generalized gradient approximation (GGA) functional PBE[3] within the Quantum Espresso suite[6]. The DFT optimization includes the Grimme[7] dispersion correction and relativistic effects up to spin-orbit couplings. For every calculation we use a plane-wave maximum cut-off energy of 90 Ry and a 2x2x2 Monkhorst-Pack[8] grid of k-points.
We assemble the final clusters from the relaxed structures as $GUACs_{19}Pb_8I_{36}$ analogue to the ones used in the previous paper by Kubicki *et al.*[1], ensuring charge compensation, high symmetry and a direct comparability of results.

EFG tensor calculation

We use the Amsterdam Density Functional (ADF)[9-10] suite to perform the EFG tensor calculation within the DFT framework. For the calculations we employ the GGA BP86[11-12] functional including the Grimme[7] dispersion correction and relativistic effects up to spin-orbit couplings within the ZORA[13-15] approximation. We use all-electron triple-ζ basis sets with two polarization functions (TZ2P)[16].
Both the cluster generation and the EFG tensor calculation are set up analogue to the previous paper by Kubicki *et al.*[1] and in accordance with recent computational studies of systems including heavy atoms.[17-21]

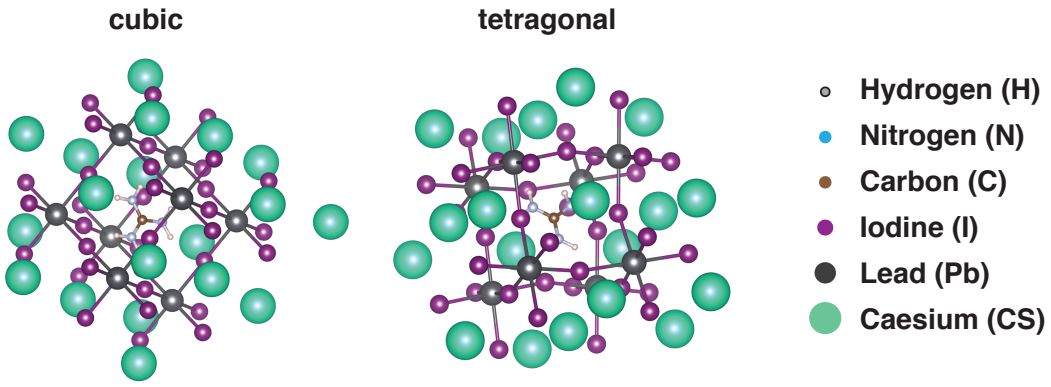

Figure S11. $GUACsPbI_3$ clusters used in the DFT EFG tensor calculations.

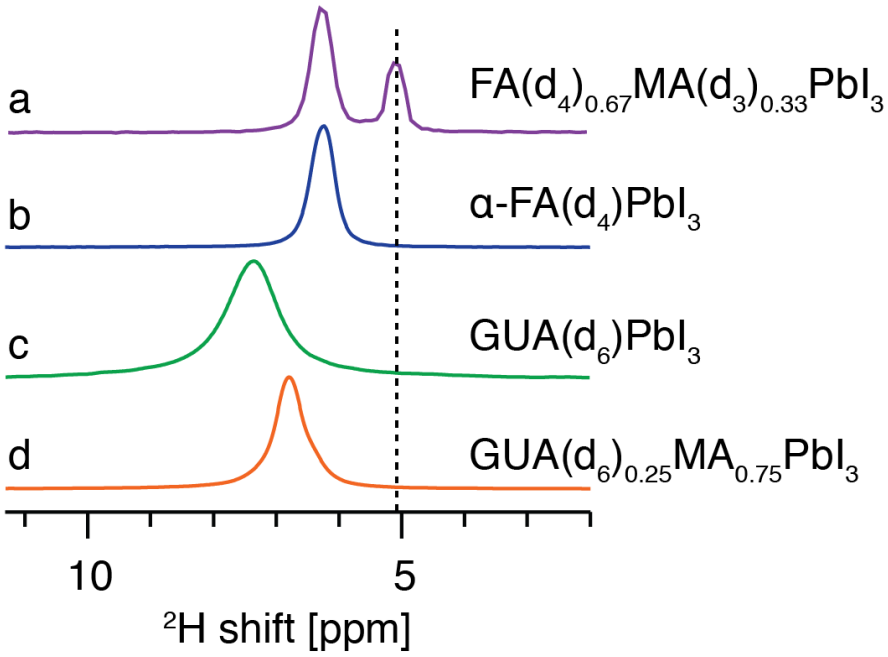

Figure S12. ^{2}H MAS NMR spectra at 11.7 T, 20 kHz MAS and 300 K of N-deuterated perovskites used as references: (a) $FA(d_4)_{0.67}MA(d_3)_{0.33}PbI_3$, and (b) α-FAPbI3, taken from previous work by Kubicki et al.[22], (c) $GUA(d_6)PbI_3$, and (d) $GUA(d_6)_{0.25}MA_{0.75}PbI_3$.

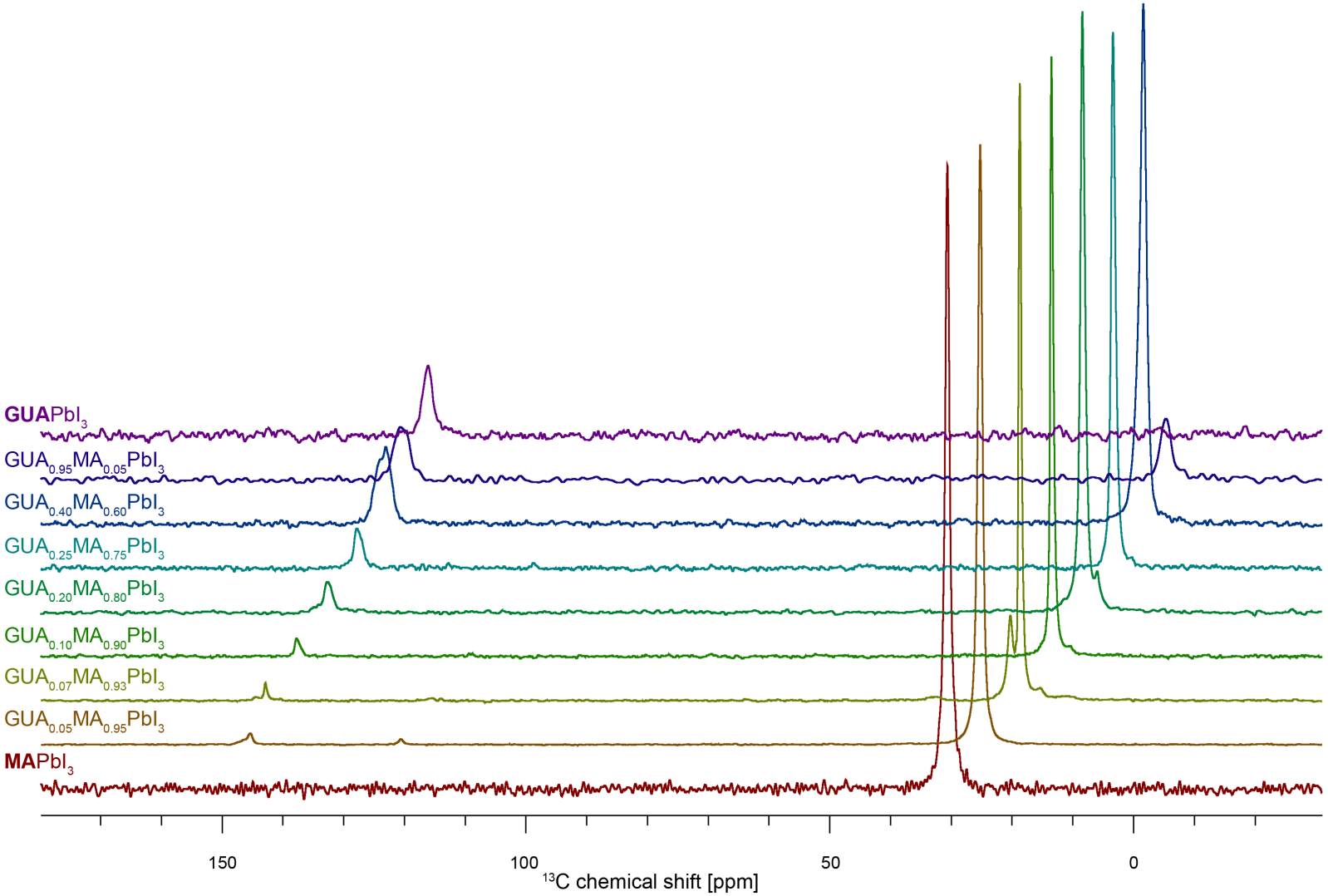

Figure S13. ^{13}C CP MAS spectra used to make fig. 1 of the main text (horizontal offset: 5.0 ppm).

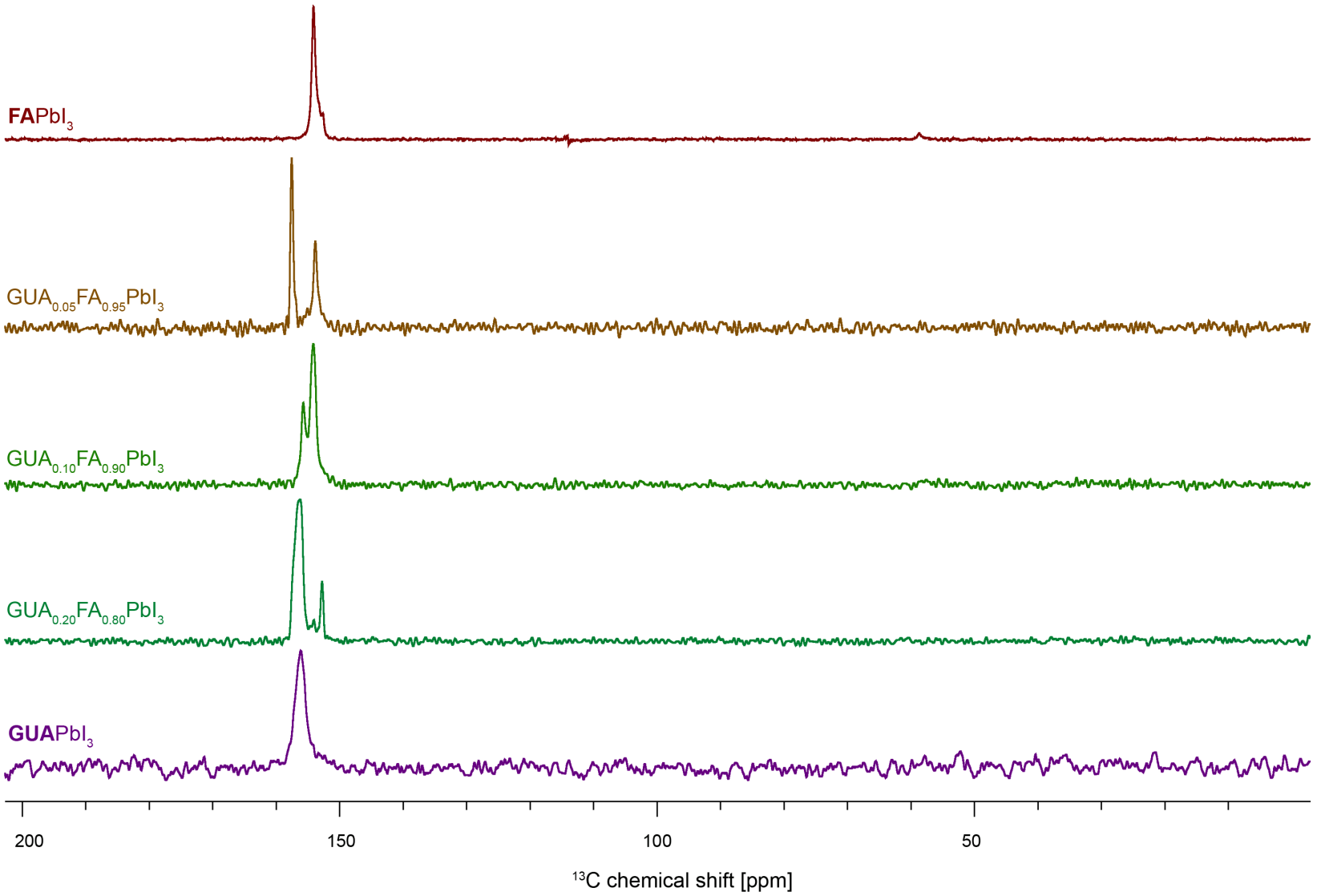

Figure S14. ^{13}C CP MAS spectra used to make fig. 1 of the main text.

Table S3. NMR acquisition parameters. References to main text and SI spectra are given in parentheses.

nucleus	# of scans	recycle delay [s]	^{1}H decoupling	RF strength [kHz]
^{13}C (CP)	300-7000 (fig. 1) 40010 (fig. S8) 41102 (fig. S9)	1-4	80 kHz SPINAL-64	100 (^{1}H)
^{2}H	45528 (fig. 2a, 100 K) 1024 (fig. 2a, 200 K) 512 (fig. 2a, 300 K) 512 (fig. 2b, 100 and 120 K) 256 (fig. 2b, 300 K)	0.1-2	-	80
^{14}N	1024 (fig. 3a, $MAPbI_3$) 2048 (fig. 3b, $FAPbI_3$) 3824 (fig. 3a, GUA/MA) 3139 (fig. 3b, GUA/FA) 145339 (fig. 3c)	0.3	-	70

References

1. Kubicki, D.; Prochowicz, D.; Hofstetter, A.; Pechy, P.; Zakeeruddin, S. M.; Graetzel, M.; Emsley, L., *The Journal of the American Chemical Society* **2017,** *139*, 10055-10061.
2. Kieslich, G.; Sun, S. J.; Cheetham, A. K., *Chemical Science* **2015,** *6*, 3430-3433.
3. Prochowicz, D.; Yadav, P.; Saliba, M.; Saski, S. M.; Zakeeruddin, S. M.; Lewinski, J.; Gratzel, M., *Sustainable Energy and Fuels* **2017,** *1*, 689-693.
4. Weller, M. T.; Weber, O. J.; Frost, J. M.; Walsh, A., *Journal of Physical Chemistry Letters* **2015,** *6*, 3209-3212.
5. Weber, D., *Zeitschrift Fur Naturforschung Section B-a Journal of Chemical Sciences* **1978,** *33*, 1443-1445.
6. Giannozzi, P.; Baroni, S.; Bonini, N.; Calandra, M.; Car, R.; Cavazzoni, C.; Ceresoli, D.; Chiarotti, G. L.; Cococcioni, M.; Dabo, I.; Dal Corso, A.; de Gironcoli, S.; Fabris, S.; Fratesi, G.; Gebauer, R.; Gerstmann, U.; Gougoussis, C.; Kokalj, A.; Lazzeri, M.; Martin-Samos, L.; Marzari, N.; Mauri, F.; Mazzarello, R.; Paolini, S.; Pasquarello, A.; Paulatto, L.; Sbraccia, C.; Scandolo, S.; Sclauzero, G.; Seitsonen, A. P.; Smogunov, A.; Umari, P.; Wentzcovitch, R. M., *Journal of Physics-Condensed Matter* **2009,** *21*.
7. Grimme, S., *Journal of Computational Chemistry* **2006,** *27*, 1787-1799.
8. Pack, J. D.; Monkhorst, H. J., *Physical Review B* **1977,** *16*, 1748-1749.
9. Guerra, C. F.; Snijders, J. G.; te Velde, G.; Baerends, E. J., *Theoretical Chemistry Accounts* **1998,** *99*, 391-403.
10. te Velde, G.; Bickelhaupt, F. M.; Baerends, E. J.; Guerra, C. F.; Van Gisbergen, S. J. A.; Snijders, J. G.; Ziegler, T., *Journal of Computational Chemistry* **2001,** *22*, 931-967.
11. Perdew, J. P., *Physical Review B* **1986,** *33*, 8822-8824.

12. Becke, A. D., *Physical Review A* **1988,** *38*, 3098-3100.
13. Vanlenthe, E.; Baerends, E. J.; Snijders, J. G., *Journal of Chemical Physics* **1994,** *101*, 9783-9792.
14. Vanlenthe, E.; Baerends, E. J.; Snijders, J. G., *Journal of Chemical Physics* **1993,** *99*, 4597-4610.
15. van Lenthe, E.; Ehlers, A.; Baerends, E. J., *Journal of Chemical Physics* **1999,** *110*, 8943-8953.
16. Van Lenthe, E.; Baerends, E. J., *Journal of Computational Chemistry* **2003,** *24*, 1142-1156.
17. Giorgi, G.; Yoshihara, T.; Yamashita, K., *Physical Chemistry Chemical Physics* **2016,** *18*, 27124-27132.
18. Alkan, F.; Dybowski, C., *Journal of Physical Chemistry A* **2016,** *120*, 161-168.
19. Dmitrenko, O.; Bai, S.; Beckmann, P. A.; van Bramer, S.; Vega, A. J.; Dybowski, C., *Journal of Physical Chemistry A* **2008,** *112*, 3046-3052.
20. Even, J.; Pedesseau, L.; Jancu, J. M.; Katan, C., *Journal of Physical Chemistry Letters* **2013,** *4*, 2999-3005.
21. Alkan, F.; Dybowski, C., *Physical Chemistry Chemical Physics* **2014,** *16*, 14298-14308.
22. Kubicki, D.; Prochowicz, D.; Hofstetter, A.; Pechy, P.; Zakeeruddin, S. M.; Graetzel, M.; Emsley, L., *J. Am. Chem. Soc.* **2017,** *139*, 10055-10061.